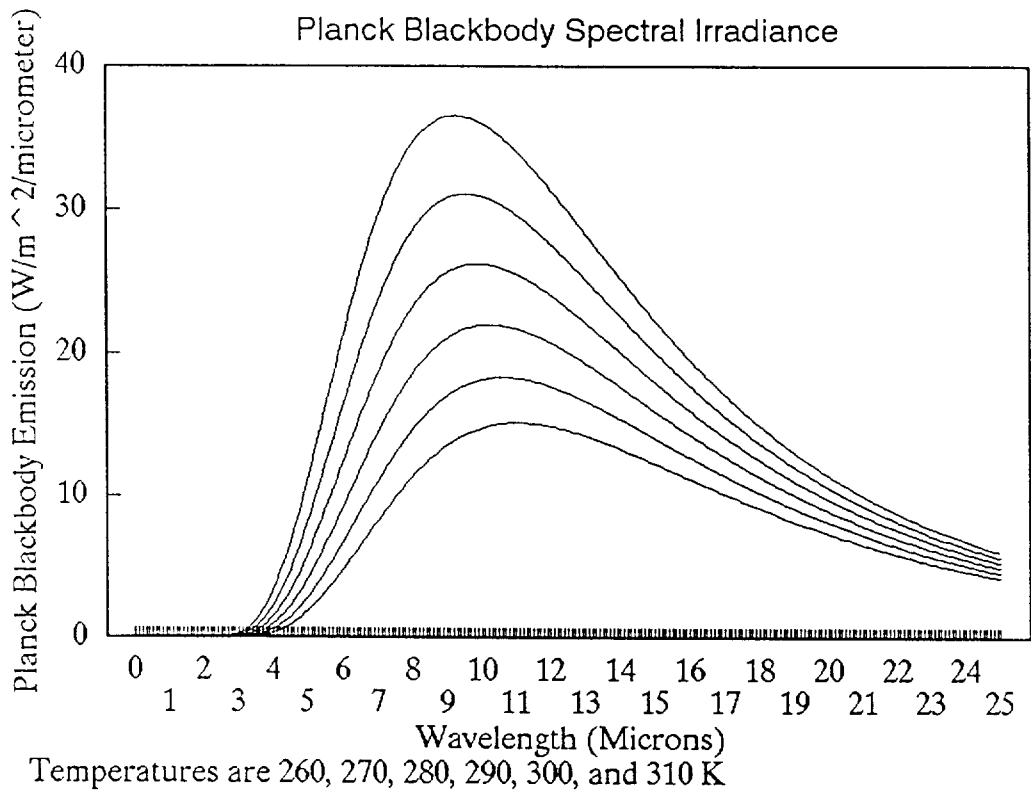


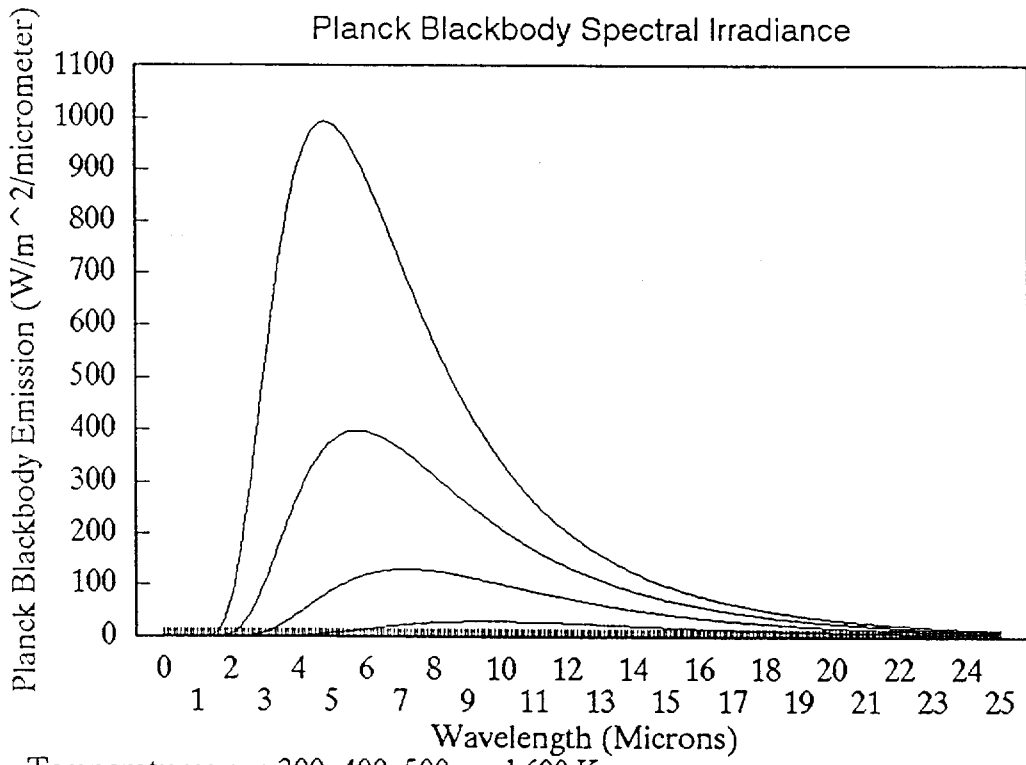
MODIS DATA STUDY TEAM PRESENTATION

October 6, 1989

AGENDA

1. Planck Spectral Blackbody Emission Curves
2. Key Earth Science Issues to be Addressed by MODIS
3. Very Preliminary Accuracies for Core MODIS Data Products and Their Relevance to the Key Earth Science Issues
4. Normalized-Difference and Soil-Adjusted Vegetation Index Algorithms
5. Snow Cover and Sea Ice Algorithms
6. Cloud Cover Algorithms
7. Maximum Likelihood Cloud Estimation Algorithm
8. Water Leaving Radiance (MODIS-Era) Algorithm
9. Case 2 Waters Pigment Concentration Algorithm
10. Surface Incident Photosynthetically Active Radiation Algorithm





Temperatures are 300, 400, 500, and 600 K

KEY EARTH SCIENCE ISSUES TO BE ADDRESSED BY MODIS

The near global daily coverage of the MODIS, combined with its continuous operation, broad spectral coverage, and relatively high spatial resolution, make it central to the objectives of Earth Observing System (Eos). MODIS data products will be required, not only by the members of the MODIS science team, but also by members of the other facility instrument teams, the interdisciplinary investigators, and the scientific community at large. The diverse observing capabilities of the MODIS-N and -T instruments allow MODIS observations and data products to be applied to many of the fundamental questions in Earth science. In particular, MODIS observations and the resultant data products will answer the following issues:

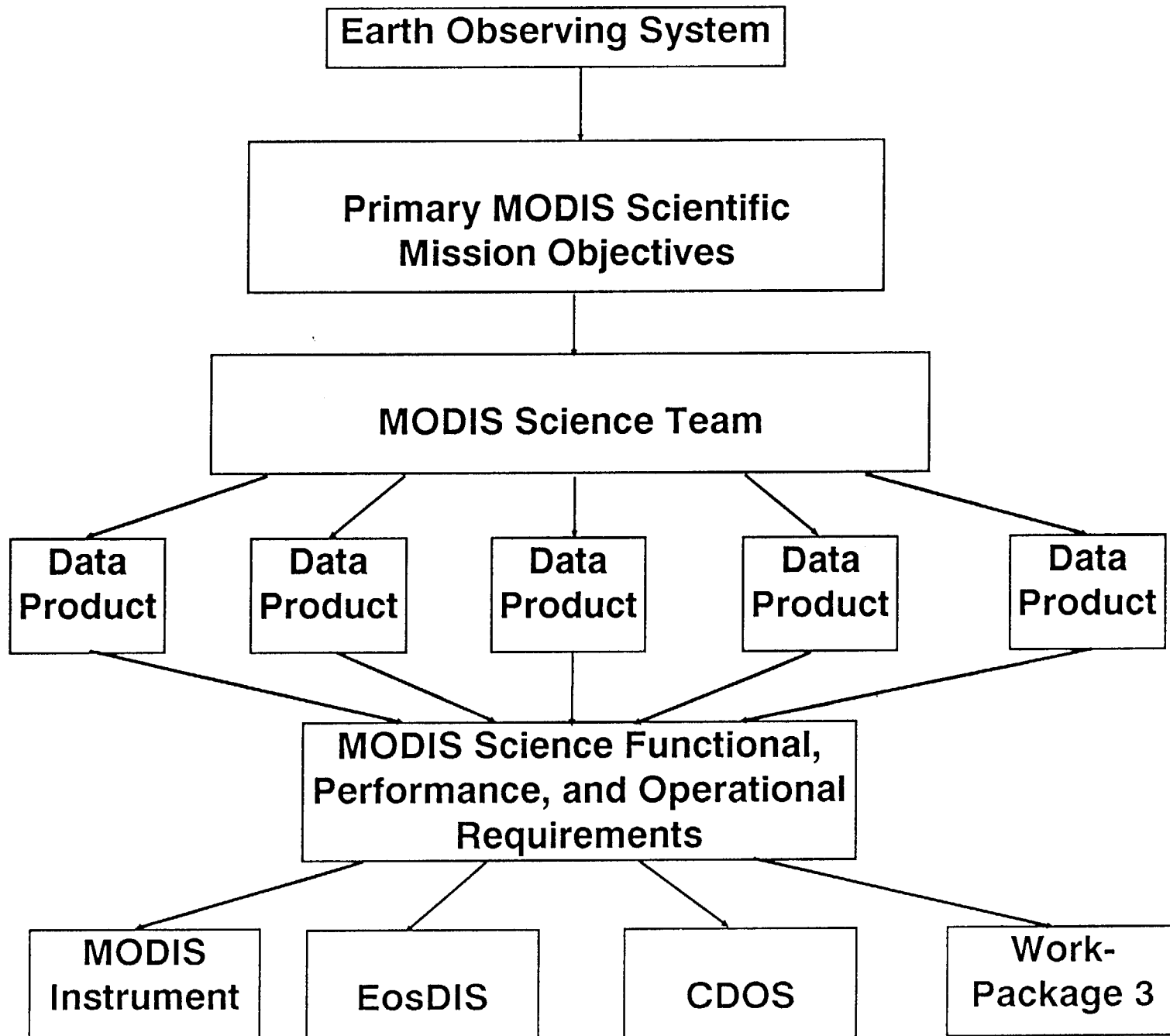
- a. Through global measurements of the photosynthetic potential of phytoplankton in the upper ocean, MODIS will allow an estimation of primary production in the upper layers of the ocean and thereby help in better understanding the process of transforming inorganic forms of carbon into organic forms and their eventual burial into deep marine sediments--an important process in the global carbon cycle.
- b. Through global measurements of the land cover and attendant estimates of photosynthetic potential or biomass, MODIS will provide observations leading to estimates of the total extent of major biomes, their variation in extent and condition over time and the relationship of these variables to the processes of deforestation, desertification, global climate changes and anthropogenic effects.
- c. Through global, relatively high spatial resolution, and long-term measurements of cloud properties including cloud type, temperature, altitude, cloud optical thickness, thermodynamic phase and effective particle radius, MODIS will provide information leading to a better understanding of the effects of clouds on the radiation budget of the Earth and the role of clouds in the so-called greenhouse warming of the Earth including associated feedback mechanisms associated with the dynamics of the atmosphere.
- d. Through measurements of snow and ice extent along with concurrent observations of surface temperature, out-going long-wave radiation, cloud cover and bi-directional reflectance obtained from MODIS, better understanding of the factors driving snow and ice melt processes over large (greater than several thousands of square kilometers, for example) watersheds, continents and the globe will be derived with subsequent better quantification of the role of these processes in the hydrological cycle.
- e. MODIS will provide fundamental observations leading to maps of evapotranspiration, photosyntheses and primary production for major biomes distributed over the Earth subsequently leading to models of surface water and carbon exchange rates by global terrestrial ecosystems.
- f. Through observations of aerosol properties on a global basis, MODIS will provide information as to the spatial and temporal variability

of aerosols and their relationship to sources and sinks associated with volcanic activity, biomass burning, anthropogenic activities and other factors associated with climate change.

The issues relate directly to the Earth's climate and global change through chemistry--the Carbon Cycle (A and B), hydrology--the Water Cycle (B and E), and the radiation and heat budget (C, D, and F).

The MODIS data study team plays a key role in analysis of the science requirements, from the primary MODIS scientific mission objectives to the system level. As illustrated, the mission requirements of the Eos and the MODIS instruments may be traced through the MODIS science team and its members to the generated set of core MODIS data products. The development, implementation, production, and validation of these core data products in turn defines a set of functional , performance, and operational requirements which must be placed on the data system, or the set of systems, that stand between the measurement taken by the sensors and the data products supplied to the user community. The primary systems include the MODIS Instrument and its processor (from sensor to data packets), Work Package 3 (from the instrument through the platform to the ground), the Customer Data and Operations System (CDOS; the Level-0 processing), and the Eos Data and Information System (EosDIS; the Level-1 through Level-4 processing).

Flow of Mission Requirements: From Science to System



AEROSOL PROCESSING OVERVIEW

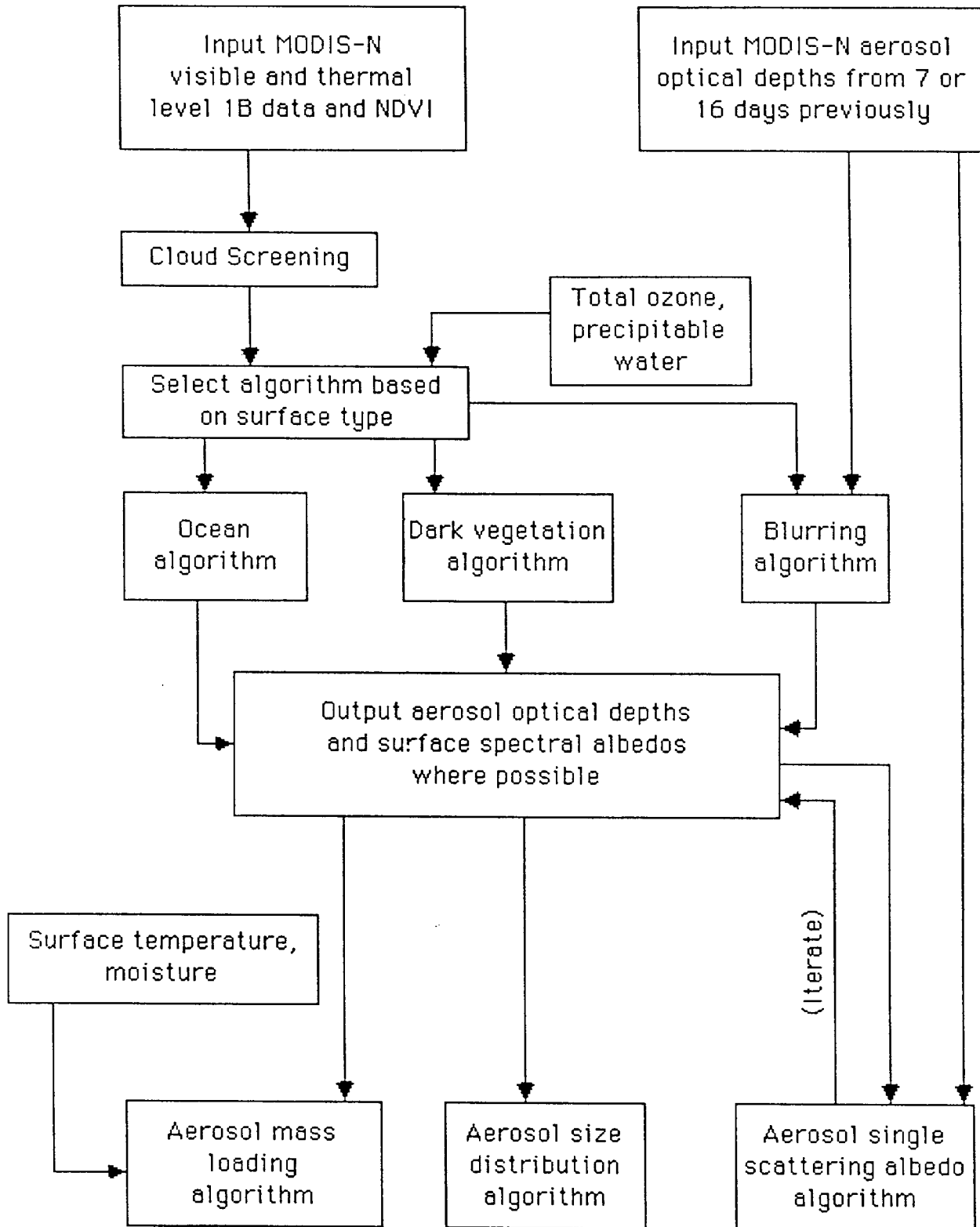
Required input to the aerosol core data product processing are Level-1B visible and thermal radiances, previously derived aerosol optical depths for scenes with the same viewing geometry, NDVI values, total column ozone amounts, total precipitable water (perhaps), and surface temperature and moisture or surface relative humidity.

The radiances are first screened to remove clouds. Depending upon the surface type, aerosol optical depth is calculated by one of three different algorithms. Surface spectral albedo will also be output from one of these algorithms.

Given the aerosol optical depths, the calculation of aerosol mass loading, aerosol single scattering albedo, and aerosol size distribution are derivative data products. Some iteration procedures may be followed to derive self-consistent answers for these aerosol properties, but the extent to which this is done is yet to be determined.

Finally it should be noted that none of these aerosol properties can be determined everywhere solely from satellite observations.

Aerosol Processing Overview



NORMALIZED-DIFFERENCE AND SOIL-ADJUSTED VEGETATION INDICES

Nature of Vegetation Indices

The fundamental physical phenomenon used to remotely identify and classify vegetation on the land surfaces of the earth involves the spectral absorption properties of chlorophyll. Chlorophyll strongly absorbs solar radiation at wavelengths below 700 nm and therefore reflects little radiation in this wavelength region. At wavelengths above 700 nm, chlorophyll absorbs little radiation and vegetation is highly reflective of solar radiation.

A number of vegetation indices have been devised, all of which make use of this fundamental physical property. Of the several indices, the one that has perhaps found the widest use is the Normalized Difference Vegetation Index (NDVI) defined as

$$NDVI = (L_{IR} - L_{red}) / (L_{IR} + L_{red})$$

where L_{IR} is the surface leaving radiance at near infrared wavelengths (upwards from 700 nm) and L_{red} is the corresponding radiance below 700 nm. If no vegetation is present and L_{IR} and L_{red} are approximately equal, the NDVI is nearly zero. If dense vegetation is present so that L_{red} is nearly zero, the NDVI approaches one. The theoretically possible values of the NDVI range from +1 to -1. The normalization (division by $L_{IR} + L_{red}$) provided with this index accounts at least approximately for varying levels of solar illumination (atmospheric effects) and effects associated with high zenith angles for observations near the edge of the instrument scan path.

A number of studies have validated the applicability of this index as a measure of vegetation activity. For illustration, a plot obtained from AVHRR data showing weekly-averages of the NDVI for the Midwestern United States is given. The index varies both with the total area covered by the vegetation (leaf area index) and with the amount and health of the chlorophyll present, i.e. healthy green vegetation is distinguishable from drought stressed or otherwise distressed or diseased vegetation that has less chlorophyll.

The primary limitation on the usefulness of the index relates to the situation where both a vegetation canopy and a soil contribute to the radiance observed by the satellite. The extent of vegetation is overestimated when light diffuses through a partial vegetative canopy and is reflected from soils lying underneath the canopy. The effect appears to result from the fact that the forward scattered radiation from the canopy is modified by the spectral characteristics of the canopy, so that the illumination incident on the underlying soil takes on some of the spectral characteristics of vegetation. Since the reflection from the soil is modified by the spectral characteristics of the incident illumination, reflections from the soil contribute to the apparent vegetation.

A Soil-Adjusted Vegetation Index (SAVI) has been proposed for use in the partial canopy situation. Although we shall not discuss the details here, the index involves the modification of the NDVI by an additive constant that depends on the extent of the vegetation canopy. The governing equation is

$$\text{SAVI} = [(L_{\text{IR}} - L_{\text{red}})/(L_{\text{IR}} + L_{\text{red}} + C)] \times (1 + C)$$

where C is an additive constant (approximately 0.25 for heavy canopies, 0.5 for moderate canopies, and 0.75 for light canopies). With this modification, it has been found that the vegetation indices depend less on the nature and properties of the underlying soil. As stated earlier, the improvement is greatest at moderate canopy densities where both vegetation and soil effects contribute to reflected radiation. For heavy canopies, the nature of the underlying soil makes little difference; for light canopies, the vegetation itself has little effect, so that the observed effect is primarily determined by the nature of the underlying soils without regard for any vegetation effects.

Implementation of the NDVI and SAVI

A possible implementation of NDVI and SAVI processing is shown. (This particular implementation is based on a previous NDVI implementation for the AVHRR). First pixel location constraints are applied to ensure that the pixel is within the required latitude interval, that the solar zenith angle is within required limits, and that the pixel is located over land. If these constraints are met, cloud screening is next applied to eliminate cloud obscured pixels. A water vapor correction may be applied, and a credibility check is made to insure the corrected radiances are greater than zero.

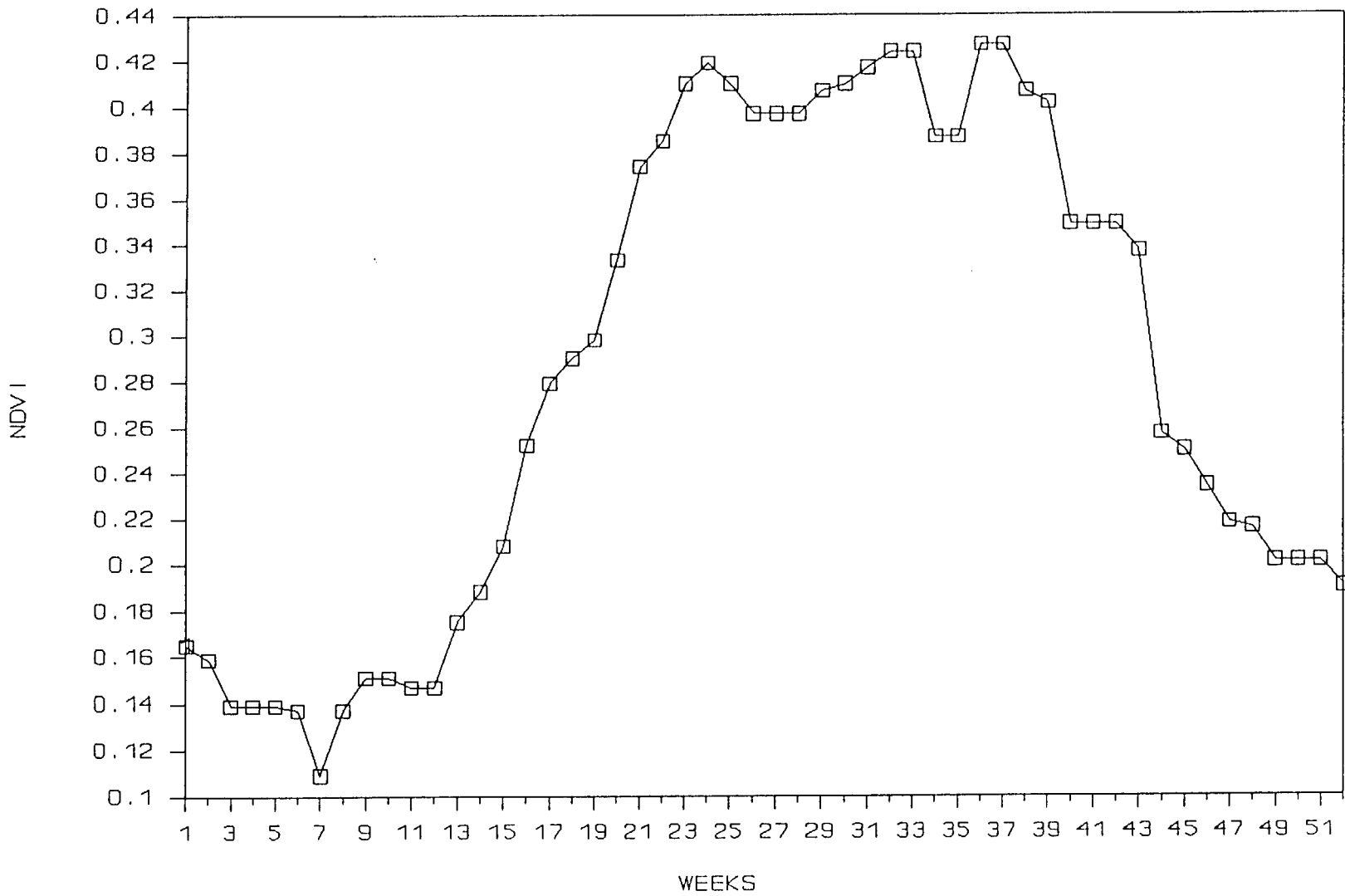
Next NDVI values are computed for each pixel using the equation given above, and for pixels with an appropriate NDVI, the SAVI is determined using canopy densities (and correction constants) based on the computed NDVI. As a part of Level-3 (earth-referenced, time and spatially averaged) processing, the processing steps may be executed to generate a synoptic picture of vegetation activity for extend regions and time periods.

References

1. Justice, C.O., Monitoring Global Vegetation Dynamics using MODIS-N, MODIS Proposal submitted to Goddard Space Flight Center, 1988
2. Huete, Alfredo R. and Ray D. Jackson, Determination of Dynamic Vegetation-Soil-Organic Carbon Interactions with MODIS Instrument Observations, Research Proposal to the National Aeronautics and Space Administration, Earth Observing System (Eos) A.O. No. OSSA-1-88, 1988
3. Huete, A.R., A Soil-Adjusted Vegetation Index (SAVI), Remote Sensing of Environment 25:295-309, 1988
4. Paltridge, G.W., and J. Barber, Monitoring Grassland Dryness and Fire Potential in Australia with NOAA/AVHRR Data, Remote Sensing of Environment 25:381-394, 1988
5. Huete, A.R., and R.D. Jackson, Soil and Atmosphere Influences on the Spectra of Partial Canopies, Remote Sensing of Environment 25:89-105, 1988.

NDVI

Midwest United States 1988



Apply Pixel Location
Tests, e.g.
|lat| < 65 Deg
Solar Angle < 85 Deg
Over Land?

Apply Cloud Screens
[e.g., IR OK?]

Perform Atmospheric
Correction (H₂O)

Radiances > 0

Compute NDVI

If partial canopy
compute SAVI

∇

To Level-3 Processing

From Level-2 Processing

V

Average over
1 deg x 1 deg region
each day

Take max value
over weekly interval

Max or median filter
over month

THERMAL ANOMALIES

Nature of Thermal Anomaly Product

High-temperature events of particular interest to the earth scientist include fires and volcanic eruptions. To a radiance measuring instrument such as MODIS these events appear as bright spots in the thermal or infrared portions of the spectrum. For a blackbody in thermal equilibrium the total thermal radiation emitted increases rapidly as the temperature of the blackbody is increased (proportional to T^4) and the wavelength of the maximum spectral density decreases as a function of temperature. The rapid increase of total thermal radiation with an increase in temperature and the characteristic shift in the shape of the spectral curve provide the identifying properties needed to distinguish high temperature or thermal anomaly events.

Since the earth's atmosphere has very low spectral transmission in several wavelength regions including the thermal infrared between about 4.5 and 8 microns, the region of peak spectral emission shown in the figure is not usually directly useful for identifying high-temperature events. However, atmospheric transmission above 8 microns and below 4.5 microns is acceptable, so that ratios between measured radiances above 8 microns and below 4.5 microns can be used to identify thermal anomaly events.

For detection of thermal anomaly events, MODIS-N provides special infrared bands at 3.750, 8.550, 11.030, and 12.020 microns. These bands are provided with a bilinear gain characteristic that extends the dynamic range of the detectors and prevents detector saturation at high temperatures. The 3.750 and 8.550 micron bands saturate at 700 degrees K and the 11.030 and 12.020 bands saturate at 400 degrees K.

The reader will readily recognize that emission in the 3.750 micron band (shown on the figure) is particularly sensitive to temperature variations within the region of interest for anomaly detection. Although the sun has a significant emission in this wavelength, an examination of the magnitude of effects shows that, for the temperatures of interest in anomaly detection, thermal emissions are much greater than solar background effects, so that this band can be used for anomaly detection day or night. Also, since absorption due to atmospheric water vapor is slight in this band, and since smoke consists largely of water vapor, smoke is atmospherically transparent in this band, so that the actual extent of fires or other thermal anomalies can be observed directly without the regions of interest being obscured by intervening smoke or other atmospheric vapors.

Implementation of Thermal Anomaly Detection

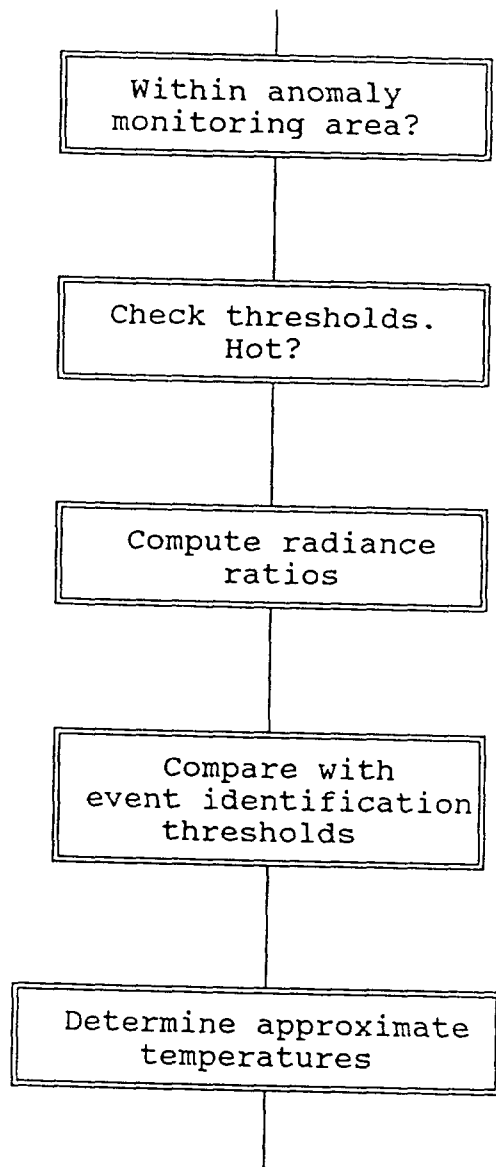
The thermal anomaly events that are of interest occur primarily over land, so that a land mask could be used to limit thermal anomaly processing to land surfaces only. However, many small islands are volcanically active, so that the usual understanding of what constitutes a land area of the earth should be carefully expanded to include all islands of potential volcanic interest. Indeed, volcanic activity is sometimes responsible for the creation of new sea islands, so that the domain of this product should perhaps be expanded to include

all ocean regions where volcanic activity could potentially create new land surfaces. This might be of particular importance since satellite remote sensing provides a ready means to monitor large areas of the earth for activity that might not otherwise be detected.

Within the domain for which the product is defined, processing might proceed roughly as shown in the figure. Presuming that surface-leaving-radiances have been generated as a part of previously applied processing (for other products), the radiances of interest might be compared with appropriate thresholds to determine if further processing for thermal anomaly is justified. For those pixels where the radiance exceeds this processing threshold, ratios of the radiance values may be computed and compared with event identification thresholds to determine the nature of the event being observed and the approximate surface temperature associated with the event.

REFERENCES:

1. Kaufman, Yoram J., Global Monitoring of Aerosol Properties - Aerosol Climatology, Atmospheric Corrections, Biomass Burning, and Aerosol Effect on Clouds and Radiation: A Proposal to be a MODIS Team Member, June, 1988
2. Stevens, George and Michael Matson, Regional and Global Fire Detection Using AVHRR Data, Proceedings of the Twenty-First International Symposium on Remote Sensing of the Environment, Ann Arbor, Michigan, October 26-30, 1987



SNOW COVER AND SEA ICE

Snowcover

The snow cover algorithm is conceptually simple. The algorithm requires a clear sky to be implemented. Then a land-ocean mask is applied to determine if the pixel is a land pixel. Two simple measurements are made (Rossow et al 1989). The surface reflectance is determined using the visible wavelengths (520 to 720nm). The infrared radiances from 10.5 to 12.5 μ m are used to determine the surface temperature. If the surface reflectance is > 35% and the surface temperature is less than 273°K, snow covers the land pixel.

It is noted that above 40°N latitude, the annual mean cloudiness exceeds 55%. From 50 to 70°N latitude the annual mean cloudiness is 64%. Consequently at least 50% of the time, no information about snow cover is available with this algorithm.

Rossow et al (1989) state that the major obstacle to global long term analysis is the lack of an effective operational technique for finding cloud free scenes in large satellite data sets. Satellite surface observations contaminated by partial cloud cover are limited in their space/time resolution.

The best cloud detection results when the less variable clear scene radiances are isolated from the satellite data. Then the clouds are identified by their alterations of the radiances. The difference between a model prediction and a radiance from a scene is interpreted as a cloud being present in the scene (Rossow et al (1989)). Once a scene is determined to be cloud free the surface properties can be determined.

When cloud detection is done by verifying the calculated clear scene radiances, this strongly implies that surface properties are well established. This is a research area. To do these surface studies the cloud detection algorithms must be tuned to eliminate all cloud containing scenes. In so doing some good clear scene data may be lost. This is necessary because a small percentage of clouds in a scene may cause changes which are much larger than surface induced changes.

It is noted that above 40°N latitude the annual mean cloudiness exceeds 55%. From 50° to 70°N latitude the annual mean cloudiness is 64% (London, 1957). Sasamori et al (1972) indicate that the cloud coverage in the southern hemisphere is at least 10% higher than for an equivalent latitude in the northern hemisphere reaching a maximum at 60°S latitude. Consequently, at least 50% of the time in the Northern Hemisphere, and about 55% of the time in the Southern Hemisphere no information is available with this algorithm.

The spectral and angular dependence of pure snow reflectances change profoundly in contrast to the behavior of soils and vegetation. The snow surface changes significantly in hours due to the temperature, winds, and aging. The Eskimos have about 100 words which describe the properties of snow. Snow's interaction with vegetation is complex; e.g., a snow fall in a forest will not remain on the trees. Consequently, surface reflectance is difficult to determine. Ground truth measurements are difficult to compare with satellite data.

Sea Ice

The sea ice algorithm is conceptually simple. The algorithm requires a clear sky to be implemented. Then a land-ocean mask is applied to determine if the pixel is an ocean pixel. Two simple measurements are then made (Rossow et al 1989). The surface reflectance is obtained using the visible wavelengths (520 to 720nm). The infrared radiances from 10.5 to 12.5 μ m are used to determine the surface temperature. If the surface reflectance is > 20% and the surface temperature is less than 271°K, sea ice covers at least 25% of the ocean pixel.

Normally mapped sea ice parameters are concentration, extent, and thickness.

Infrared and visible sea ice information will show the sea ice extent but no information concerning its thickness (or age). The sea ice extent which is satellite mapped depends upon the sea ice concentration. The sea ice concentration is the percentage of the ocean which is covered with sea ice. It has been expressed in tenths or eights. The sensor resolution determines the minimum sea ice concentration which is seen. Field experience indicates when the sea ice concentration is less than 30% satellite images are difficult to interpret. A ship will report that sea ice is present, but the satellite doesn't detect it. This is one factor which causes differences between satellite derived sea ice boundaries and those obtained by surface or aircraft observations.

Sea ice thickness is a measure of the sea ice age. One year old sea ice is about one meter thick. Sea ice older than one year (such as found in the Arctic Ocean) is about two to three meters thick. The multi-year extent will obviously have an important influence on ship routing. Only the most powerful icebreakers can force a passage through Arctic Ocean sea ice.

The surface configuration and roughness is a function of whether the sea ice is forming or melting. Since sea ice moves under the influence of the wind, older sea ice will display rafting where one ice flow has overridden another either partially or totally. These surfaces will be very irregular. Newly formed sea ice will tend to be smooth. Little climatological information is available for sea ice reflectance to quantify this.

Sea ice ridges tend to form in days and to deteriorate in months. Sea ice ridges may extend 10 meters out of the water with a keel which is 30 to 40 meters. These features will stop ships. An icebreaker can't go through them. Their detection would be very useful to ship routing or resupply operations.

Although sea ice moves under the influence of the wind and ocean currents, it tends to be persistent in a given location. Sea ice edges may be detected from cloud covered satellite images because the same feature, or a similar feature will appear on successive images while the clouds tend to move. This technique will most likely require human intervention with MODIS products.

It is noted that above 40°N latitude the annual mean cloudiness exceeds 55%. From 50° to 70°N latitude the annual mean cloudiness is 64% (London, 1957). Sasamori et al (1972) indicate that the cloud coverage in the southern hemisphere is at least 10% higher than for an equivalent latitude in the northern hemisphere reaching a maximum at 60°S latitude. Consequently, at least 50% of the time in

the Northern Hemisphere, and about 55% of the time in the Southern Hemisphere no information is available with this algorithm.

The implication is that the cloud detecting algorithm is as important to this product as the algorithm used to detect sea ice.

REFERENCES

Rossow, W.B., C.L. Brest, and L.C. Garder
Global, Seasonal Surface Variations from Satellite Radiance Measurements
Journal of Climate, Vol. 2. March 1989, pp 214 -247.

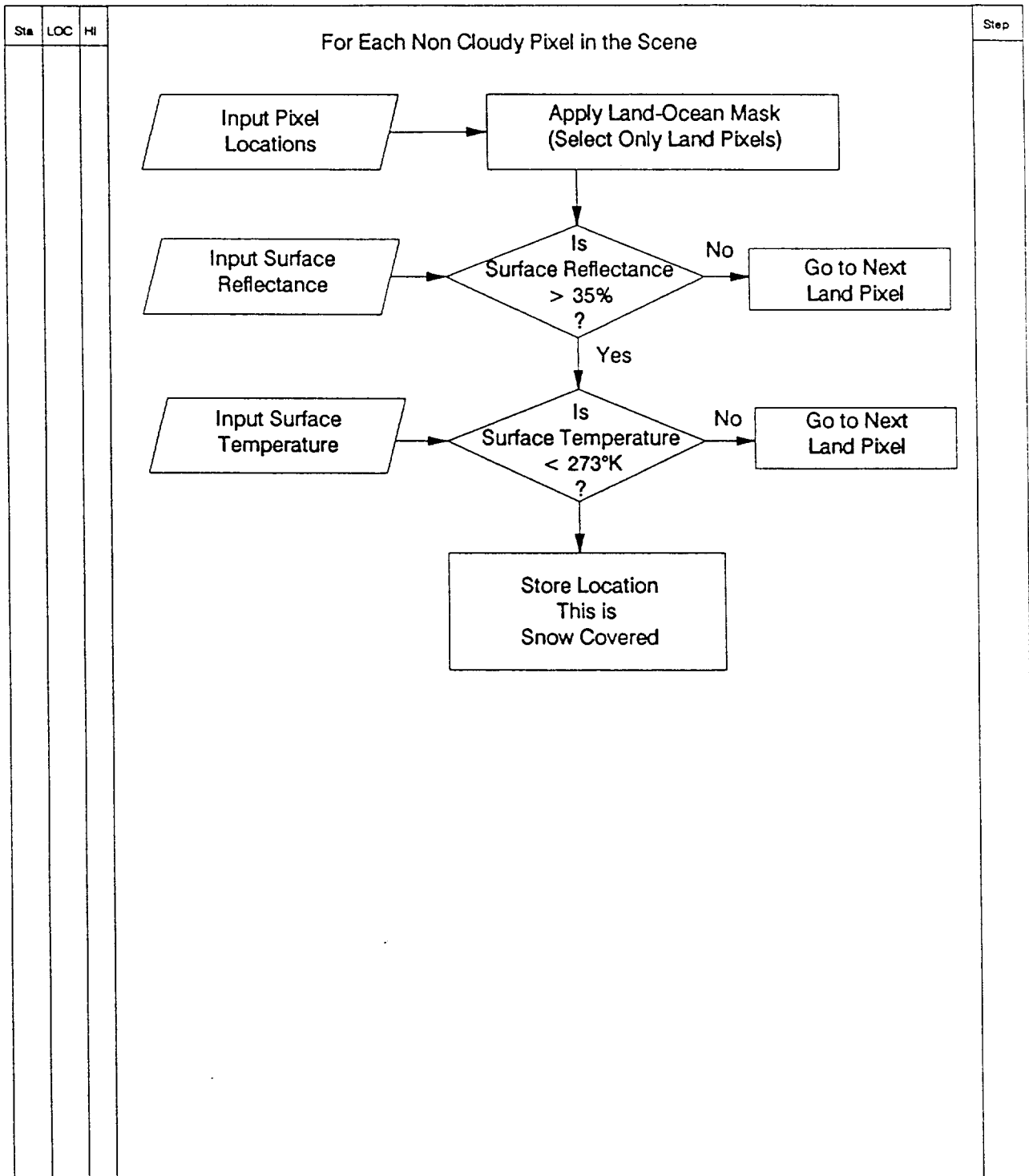
Rossow, W.B., L.C. Garder and A.A. Lacis
Global, Seasonal Cloud Variations from Satellite Radiance Measurements. Part
1: Sensitivity of Analysis.
Journal of Climate, Vol. 2 , May 1989 pp. 419-458.

London, J.
A Study of the Atmospheric Heat Balance. Final Report
Contract No. AF 19(122)-165, New York University, 1957

Sasamori, T, J. London, and D. Hoyt
Radiation Budget of the Southern Hemisphere
Meteorology Monographs
Meteorology of Southern Hemisphere
American Meteorology Society 1972

Snow Cover

Global Seasonal Cloud Variations from Satellite Radiance Measurements. Part 1: Sensitivity of Analysis
 Rossow, W. B., L.C. Garder, and A.A. Lacis
 Journal of Climate, Vol. 2, May 1989, pp. 419 - 458.

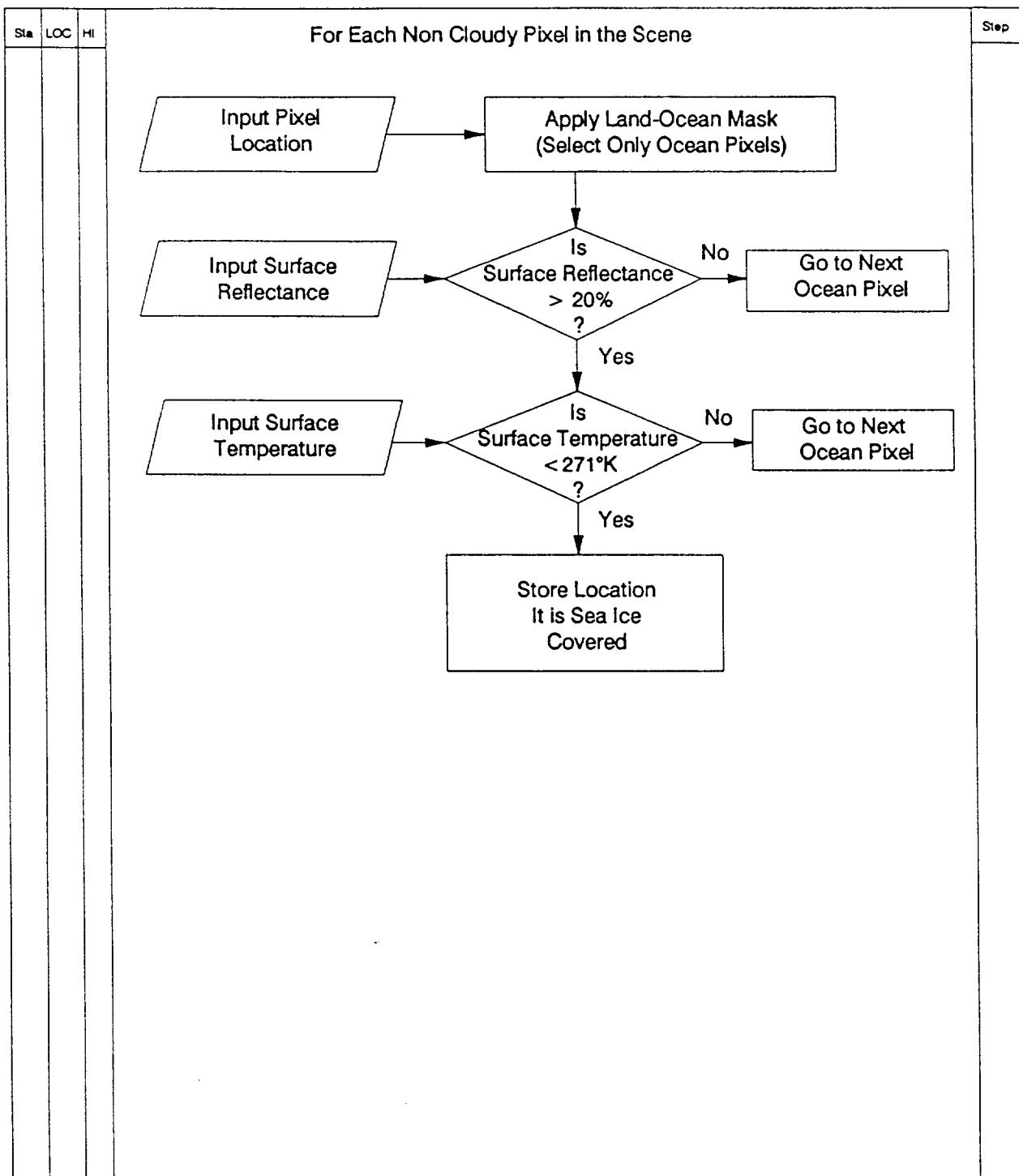


Legend: Sta = Algorithm Status HI = Current Human Intervention
 O - Operational A - Autonomous
 D - Development H - Some Human
 C - Conceptual M - All Manual
 LOC = Lines of Code

Oct 4, 1989

Sea Ice

Global Seasonal Cloud Variations from Satellite Radiance Measurements. Part 1: Sensitivity of Analysis
 Rossow, W. B., L.C. Garder, and A.A. Lacis
 Journal of Climate, Vol. 2, May 1989, pp. 419 - 458.



Legend: Sta = Algorithm Status
 O – Operational
 D – Development
 C – Conceptual
 LOC = Lines of Code

HI = Current Human Intervention
 A – Autonomous
 H – Some Human
 M – All Manual

Oct 4, 1989

CLOUD-COVER ALGORITHMS

For the analysis and retrieval of data products at the Earth's surface, it will be necessary to identify the presence of clouds. Cloud identification and atmospheric correction algorithms must occur at an earlier level than the generation of most data products because these procedures are required for the generation of most Level-2+ products. The cloud identification algorithms to be employed at the beginning of Level-2 processing are for the most part unrelated to the algorithms that will create the core Level-2 cloud products. The core cloud product algorithms will be more sophisticated than those required to make a yes/no decision regarding cloud cover. Furthermore, there are a substantial number of techniques available that may be used for the identification of cloud cover.

The MODIS instruments, and particularly MODIS-N, offer a wide spectral capability for cloud detection. Algorithms based on the shortwave reflected radiation, the near-IR, and the thermal IR may be utilized. Because many of the Level-2 data product algorithms have a heritage that is distinct and unique from the other product algorithms, it will be necessary to employ multiple (parallel) cloud detection algorithms. A set of flags (from six to ten) will be set based on the detection technique (e.g., IR threshold, VIS reflectance, spectral flatness, spatial coherence, bispectral, maximum likelihood, etc.). This processing will occur at the very beginning of the Level-2 processing.

Candidate Cloud Detection Procedure

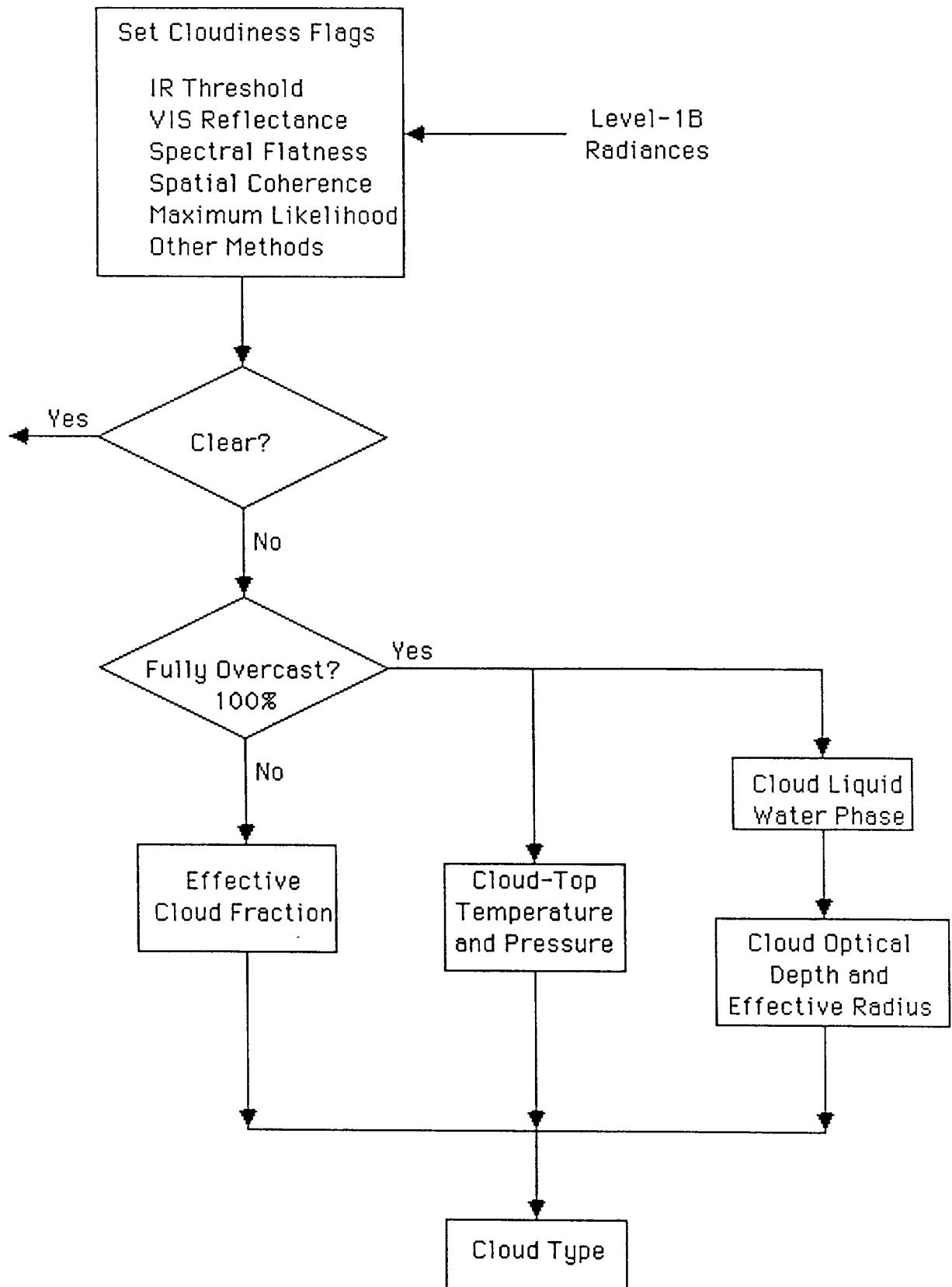
The first step in the Level-2 processing of the MODIS-N data may be the identification of pixels containing clouds. There are several methods of detecting clouds. A fully automated method for cloud detection in AVHRR data will be presented as an example of how clouds might be detected by MODIS-N. The AVHRR method is presented by Saunders and Kriebel, 1988. The basic idea is to divide the pixel into three classes: clear, cloudy, and mixed. The clear pixel should be completely clear, i.e., no detectable clouds. The cloudy pixels should be 100% covered with homogenous clouds. The rest of the pixels are classified as partly cloudy.

The classification of clear pixels is done by applying a series of 5 simple tests for clouds. A pixel is flagged as cloud contaminated if any single test is passed. Different tests are used for daytime and nighttime data. The day test use channels 1 and 2 visible albedos plus 11 and 12 μm brightness temperature. At night, the 3.7 μm NIR channel is used instead of the visible channels. The series of tests is illustrated in Figure ***&

The first test, applied both day and night, is an infrared threshold test at 12 μm . This flags the cold pixels as cloud contaminated. The second test is based on spatial coherence and is applied globally at night and over the ocean during the day. The standard deviation is calculated on a 3 x 3 array of 11 μm brightness temperature. Those pixels which have large standard deviations are flagged as cloud contaminated.

The third test is a visible threshold test which is applied only when the solar elevation is larger than 10°. Those pixels which are brighter than the threshold

Cloud Core Product Processing Overview



are flagged. A dynamic threshold is used based on surface type. The fourth test is based on the ratio NIR/VIS radiance. The pixel is flagged if the ratio is less than 1.6 over land or greater than 0.75 over sea.

The fifth test detects thin cirrus and is applied both day and night. The difference in the brightness temperatures at 11 and 12 μm are compared to a threshold value which is determined by the 11 μm temperature and the satellite zenith angle. Those pixels with "large" differences are flagged.

The third and fourth test at night are also based on difference thresholds. The third test flags those pixels for which $T(11) - T(12)$ exceeds 1.0°K . The fourth test sets the flag if $T(3.7) - T(12)$ is larger than 1.5°K .

It has been shown that this set of test does allow only clear pixels to fail the entire set of tests. There will be some clear pixels flagged as cloud contaminated when there is large variation in the surface coverage, e.g., coastal areas.

The pixels which are flagged as cloud contaminated have two additional tests applied. The first test sets a threshold of 1.0°K on the standard deviation calculated in test two above. If the standard deviation is too large the pixel is flagged as partly cloudy.

The second daytime test requires that the NIR/VIS ratio be "close to" 1. If not, the pixel is partly cloudy. At night, the pixel is flagged as partly cloudy if $T(11) - T(3.7) > 1.5$ or $T(11) - T(12)$ is less than the threshold value used in the thin cirrus test. (This last test has the consequence of flagging pixels with thin cirrus clouds as partly cloudy at night. This appears to be an unavoidable consequence of the problems of observing cirrus clouds with IR data only.)

This scheme was optimized for use with AVHRR and it is likely that the set of tests could be modified and/or expanded for use with MODIS-N. There are several advantages to this technique. First, this technique can be applied to an individual MODIS swath. Second, the tests are simple; relatively few calculations are required. Atmospheric corrections are not needed and surface type is the only required ancillary data. Finally, the pixels are divided into three classes that are appropriate for further analysis. The clear pixels are really clear and the cloudy pixels will have relatively homogenous cloud cover.

A bi-spectral clustering technique has been described by Arking and Childs and extended to three dimensions by Desbois, Seze, and Szejwach. This technique uses a scene of data, typically a square 250 km on a side. The bi-spectral method uses visible and infrared bands with the 3-D method adding a water vapor channel. The observed radiance (or temperature) is then plotted.

The areas of the scene that contain uniform coverage of either clouds or surface type will generate clusters in the plots. Automated techniques have been developed to identify the clusters. Points outside the clusters are assumed to have partial cloud coverage. The absolute cloud fraction can be estimated based

on how far the individual pixels are from the clusters. The 3-D method is capable of making distinctions between cloud and surface types that cannot be done in the bi-spectral method.

The clustering method has the advantage that it works without any a priori knowledge. The scene is analyzed based only on the clustering on the observed data. This method has two disadvantages. First, it requires a very large amount of computation to properly determine how the data is clustered. Second, it requires large square scenes. For MODIS, this technique would require combining swaths and reformatting the data.

SURFACE INCIDENT PHOTOSYNTHETICALLY ACTIVE RADIATION

Introduction

Estimates of the surface incident photosynthetically available (active) radiation (PAR) are critical for determining the photosynthetic rates of growth of oceanic phytoplankton, and thus their primary production. PAR is defined as

$$\text{PAR} = 1/hc_s \int_{400}^{700} \lambda E_d(\lambda) d\lambda, \quad (1)$$

where h is Planck's constant, c_s is the speed of light, and $E_d(\lambda)$ is the downwelling irradiance expressed as the flux of energy.

Probably the best methods for computing broad-band total insolation (which can then be converted to PAR) are those of Gautier et al. (1980) and Dedieu et al. (1987). Both are based on fundamental physical principles and utilize satellite data. Accuracies are very good; Gautier and Katsaros (1984) reported a standard deviation of 13 W m^{-2} between the Gautier et al. (1980) model and observations. Another advantage of the models is that, because they use high repeat coverage satellite data, they can compute irradiance at 1/2 hour intervals, and thus directly determine the temporal variability of clouds, the major atmospheric constituent affecting surface PAR. At horizontal resolutions of 1 km^2 and 25 km^2 respectively for the Gautier et al. (1980) and Dedieu et al. (1987) models, spatial variability can be determined from their models as well.

Unfortunately, these models require an exorbitant amount of data and are thus considered unsatisfactory for MODIS processing requirements (Wayne Esaias, personal communication). One would expect the LOWTRAN or 5S models to be equally unacceptable. Other, less computationally expensive, methods must be sought.

Since a specific method has not been proposed for the MODIS processing effort, we shall discuss a few possibilities, their strengths and weaknesses. Most of these methods rely on models, which can utilize either atmospheric data obtainable from MODIS or other sources, or representative atmospheres.

A number of clear (cloudless) sky models are available (e.g., Seckel and Beaudry, 1973; Justus and Paris, 1985; Bird and Riordan, 1986; Gregg and Carder, 1989; also see Iqbal, 1983), although only one (Gregg and Carder, 1989) is specific for maritime atmospheres.

The major problem in determining PAR, however, is clouds, which drastically affect the downwelling PAR but whose effects are extremely difficult to quantify. Their distributions in time and space are also extremely variable, which further complicates the quantification of their effects. Because of the uncertainty related to cloud effects and distribution, and because clouds are the dominant atmospheric constituent affecting downwelling PAR (much greater than Rayleigh scattering, aerosols, and ozone), the estimations of PAR are likely to contain substantial error. A number of cloudy sky models have been developed (see Iqbal, 1983), which are primarily statistical and have different averaging periods (daily, monthly, yearly). Below we have selected three methods that are specific

for maritime environments, which can depend on MODIS output products. All the methods suggested below will require (and depend substantially upon) some means of estimating temporal and spatial variability of clouds.

Direct Measurements of Reflectance from MODIS

This method attempts to deduce downwelling surface irradiance from the radiance detected at the satellite. For cloudy skies, one may assume that all the radiance received at the satellite is due to clouds. For a given wavelength within the range of PAR, i.e., 550 nm, and assuming a Lambertian radiance distribution

$$R(\lambda) = \pi L_c(\lambda)/F_o(\lambda) \quad (2)$$

where $L_c(\lambda)$ = radiance due to clouds = $L_t(\lambda)$, the total radiance at the sensor, and $F_o(\lambda)$ is the instantaneous extraterrestrial irradiance. Since clouds do not absorb in the visible (i.e., within the PAR range),

$$E_d(\lambda,0) = F_o(\lambda) [1 - R(\lambda)] \quad (3)$$

where $E_d(\lambda,0)$ is the irradiance penetrating the cloud and impinging on the surface, excluding other atmospheric optical effects.

By Eqn. 1, PAR may be computed as the integral of $E_d(\lambda,0)$ over λ , or, by noting that cloud reflectance is independent of λ , we may derive

$$PAR = (1 - R)/hc_s \int \lambda F_o(\lambda) d\lambda \quad (4)$$

Thus an approximate expression for surface PAR is obtainable under clouds directly from MODIS. This method is likely to overestimate PAR for clear pixels, since no other atmospheric attenuation has been included and is necessary in the absence of clouds. For clear pixels, a radiative transfer model including these atmospheric constituents will have to be employed to obtain PAR.

Advantages: obtain PAR under cloudy skies directly from MODIS, computationally cost-effective

Disadvantages: requires clear sky model, unvalidated, requires a method to extrapolate/interpolate temporal and spatial cloud variability.

Model of Gregg and Carder (1989)

This model has been validated for typical cloudless, maritime atmospheres (those dominated by marine aerosols) with excellent results ($\pm 3.5\%$). It computes high spectral resolution (1 nm) irradiance over 350-700 nm, and computation of PAR is a simple matter of integration. It computes the directionality of the irradiance (direct or diffuse), which has been shown to be important for transmittance of light in the water column. The model thus provides a reasonably accurate estimate of cloudless irradiance

$$E_d(\lambda, 0^-) = F_o(\lambda) \exp[-(\tau_r L + \tau_{oz} L_{oz})] \\ \times [\exp(-\tau_a L)(1-\rho_s) + 0.85D(1-\rho_d)] \quad (5)$$

$$D = 0.5[\exp(0.8\tau_r L) - 1] + F_a[1 - \exp(-\omega_a \tau_a L)] \quad (6)$$

where λ -dependences have been suppressed. $E_d(\lambda, 0^-)$ is the downwelling irradiance just below the sea surface, $F_o(\lambda)$ is the extraterrestrial irradiance corrected for Earth-Sun orbital distance and orbital eccentricity, $\tau_r(\lambda)$ is the Rayleigh optical thickness, $\tau_{oz}(\lambda)$ is the ozone optical thickness, $\tau_a(\lambda)$ is the aerosol optical thickness, $\omega_a(\lambda)$ is the single scattering albedo of the aerosol, $F_a(\theta)$ is the aerosol forward-scattering probability, $L(\theta)$ and $L_{oz}(\theta)$ are the slant path lengths through the atmosphere for Rayleigh/aerosols and ozone, respectively, $\rho_s(\theta)$ is the direct sea surface reflectance, and ρ_d the diffuse reflectance. The model computes the direct irradiance if D is set to zero, and the diffuse irradiance if $\exp(-\tau_a L)$ is set to zero. As shown it computes the global (direct and diffuse) irradiance. PAR is computed by Eqn. 1.

Although the model was developed using typical, representative atmospheric characteristics, many (such as τ_r , τ_{oz} , τ_a) will be available for MODIS for specific locations and times, and should increase the accuracy of Eqs. 5 and 6.

The problem arises with cloud cover, for which the model was not designed. However, if a few cloud parameters can be determined, the model should be able to compute the effects of clouds on instantaneous irradiance, and Eqs. 5 and 6 can easily be modified to include these effects

$$E_d(\lambda, 0^-) = F_o(\lambda) \exp[-(\tau_r L + \tau_{oz} L_{oz})] \\ \times [\exp(-\tau_a L + \tau_c L)(1-\rho_s) + 0.85D(1-\rho_d)] \quad (7)$$

$$D = 0.5[\exp(0.8\tau_r L) - 1] + F_a[1 - \exp(-\omega_a \tau_a L)] \\ + F_c[1 - \exp(-\tau_c L)] \quad (8)$$

Thus the cloud parameters required are cloud optical thickness τ_c , and the probability of forward scattering for clouds F_c . The cloud optical thickness can be obtained from the MODIS cloud products, but F_c is more difficult. Estimates of F_c may be derived if the cloud droplet size distribution (a MODIS core data product) is known.

The method produces only instantaneous irradiance, hence daily cloud cover will require a temporal averaging scheme.

Advantages: high accuracy of clear sky irradiance ($\pm 3.5\%$), expected higher accuracy with input from MODIS products, specificity for PAR and marine conditions, high spectral resolution, directionality of irradiance, derivation from fundamental physical principles, computationally cost-effective.

Disadvantages: forward scattering probability and single scattering albedo of

aerosols will have to be estimated, and forward scattering probability of clouds probably requires a multiple scattering computation, requires knowledge of spatial and temporal variation of clouds, unknown accuracy of cloud effects.

Model of Kuring et al. (1989)

This method obtains surface PAR using satellite determined estimates of cloud cover. Clear sky irradiance for total insolation (flux of energy) Q_{cs} is known from

$$Q_{cs} = A_0 + A_1 \cos\phi + B_1 \sin\phi + A_2 \cos(2\phi) + B_2 \sin(2\phi) \quad (9)$$

(Seckel and Beaudry, 1973) where ϕ is the sun angle defined by $\phi = (\text{Julian Day} - 21) \times 360/365$. The coefficients A_1 and B_1 are empirical functions of latitude.

Percent cloudiness C is determined from Level 3 CZCS data (compressed Earth gridded data set) by

$$C = 100F/N \quad (10)$$

where N is the total number of original CZCS pixels in the compressed gridded pixel, and F is the number of original CZCS pixels flagged because of land or clouds.

Measurements of the ratio R of measured irradiance to the clear sky irradiance Q_{cs} were regressed against C to produce a relationship between the satellite-determined C and the measured R . Then $Q_{cs} \times C$ yielded the irradiance. This computed irradiance was multiplied by $0.397 \text{ Ein W}^{-1} \text{ day}^{-1}$ to convert energy flux into quantum flux $\text{Ein m}^{-2} \text{ day}^{-1}$, and then multiplied by 0.46 (Baker and Frouin, 1987) to convert to PAR (350-700 nm).

Advantages: PAR can be computed from MODIS, thereby avoiding problems of co-location and temporal registering required if data from other satellites are used, reasonable accuracy (standard deviation of $\pm 21 \text{ W m}^{-2}$), and computational efficiency.

Disadvantages: reduced accuracy relative to other methods, and a requirement of in-situ measurements (at least once, over season and location) from which to develop a relationship between C and R . Requires a means to estimate temporal and spatial cloud cover.

References

Baker, K.S. and R.F. Frouin, 1987. Relation between photosynthetically available radiation and total insolation at the ocean surface under clear skies. *Limnology and Oceanography* 32: 1370-1377.

Bird, R.E. and C. Riordan, 1986. Simple solar spectral model for direct and diffuse irradiance on horizontal and tilted planes at the Earth's surface for cloudless atmospheres. *Journal of Climate and Applied Meteorology* 25: 87-97.

Dedieu, G., P.Y. Deschamps, and Y.H. Kerr, 1987. Satellite estimations of solar irradiance at the surface of the earth and of surface albedo using a physical model applied to Meteosat data. *Journal of Climate and Applied Meteorology* 26: 79-87.

Gautier C., G. Diak, and S. Masse, 1980. A simple physical model to estimate incident solar radiation at the surface from GOES satellite data. *Journal of Applied Meteorology* 19: 1005-1012.

Gautier, C. and K.B. Katsaros, 1984. Isolation during STREX. 1. Comparisons between surface measurements and satellite estimates. *Journal of Geophysical Research* 89: 11779-11788.

Gregg, W.W. and K.L. Carder, 1989. A simple, very high spectral resolution solar irradiance model for cloudless maritime atmospheres. *Limnology and Oceanography*, submitted.

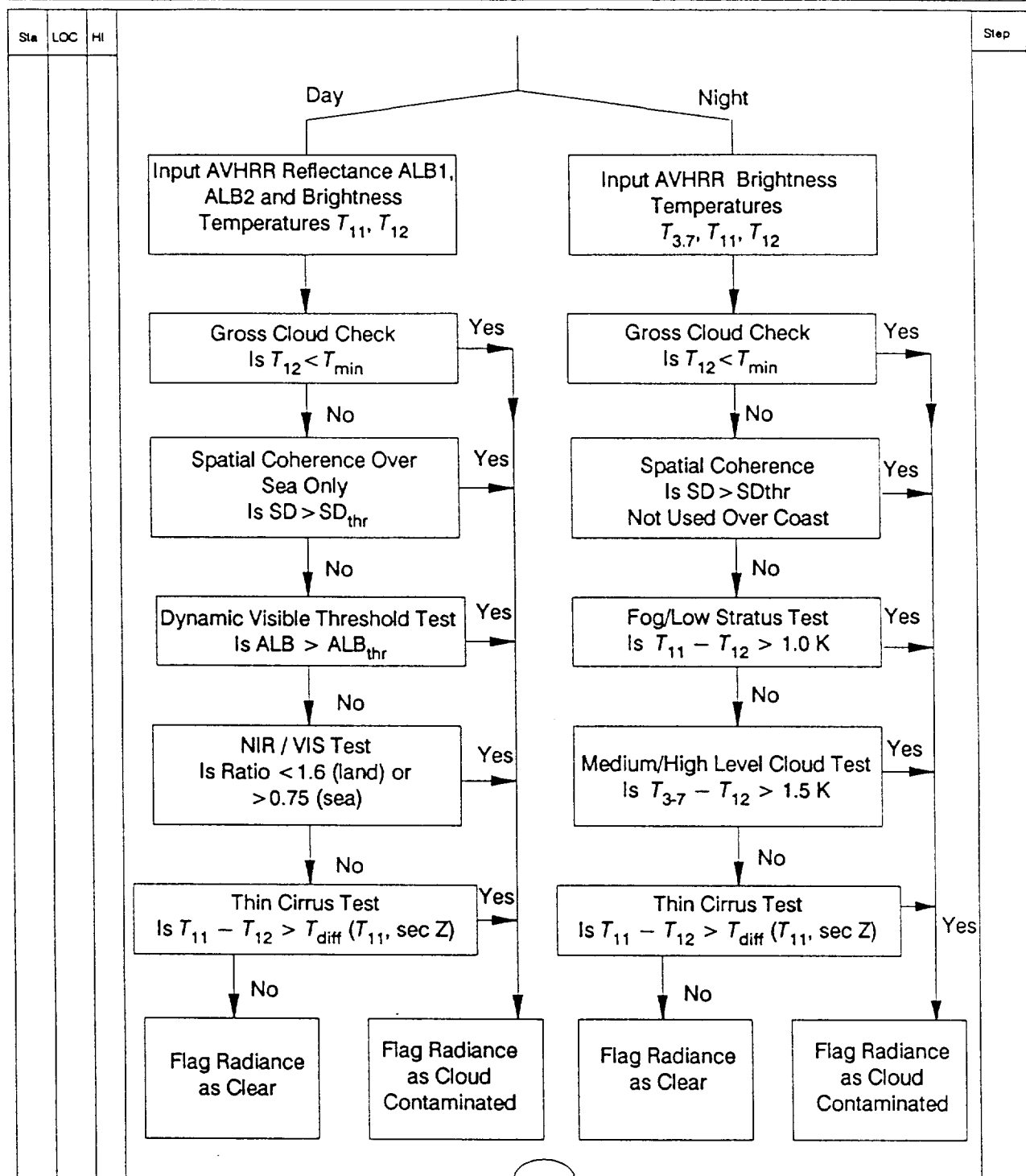
Iqbal, M., 1983. An introduction to solar radiation. Academic Press, New York. 390 pp.

Justus, C.G. and M.V. Paris, 1985. A model for solar spectral irradiance and radiance at the bottom and top of a cloudless atmosphere. *Journal of Climate and Applied Meteorology* 24: 193-205.

Kuring, N., M.R. Lewis, T. Platt, and J.E. O'Reilly, 1989. Satellite derived estimates of primary production on the northwest Atlantic continental shelf. *Continental Shelf Research*, in press.

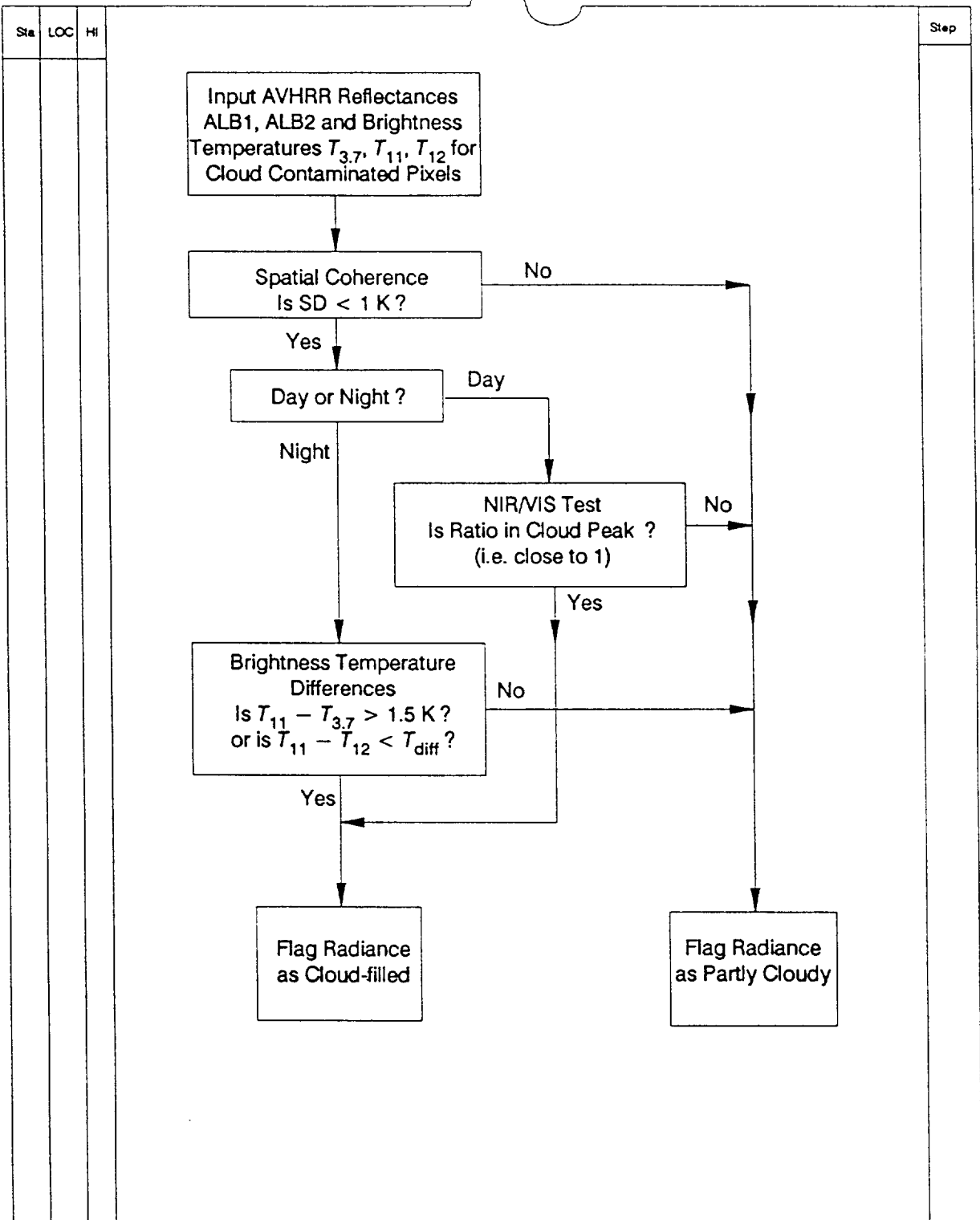
Seckel, G.R. and F.H. Beaudry, 1973. The radiation from sun and sky over the North Pacific Ocean (abstract). *Transactions of the American Geophysical Union* 54: 1114.

AVHRR Pixel Classification Procedure – I. Clear Pixels
(Ref: Saunders & Kriebel)



Legend: Sta = Algorithm Status
 O – Operational
 D – Development
 C – Conceptual
 LOC = Lines of Code
 HI = Current Human Intervention
 A – Autonomous
 H – Some Human
 M – All Manual

AVHRR Pixel Classification Procedure – II. Cloud Filled Pixels



Legend: Sta = Algorithm Status
 O – Operational
 D – Development
 C – Conceptual
 LOC = Lines of Code
 HI = Current Human Intervention
 A – Autonomous
 H – Some Human
 M – All Manual

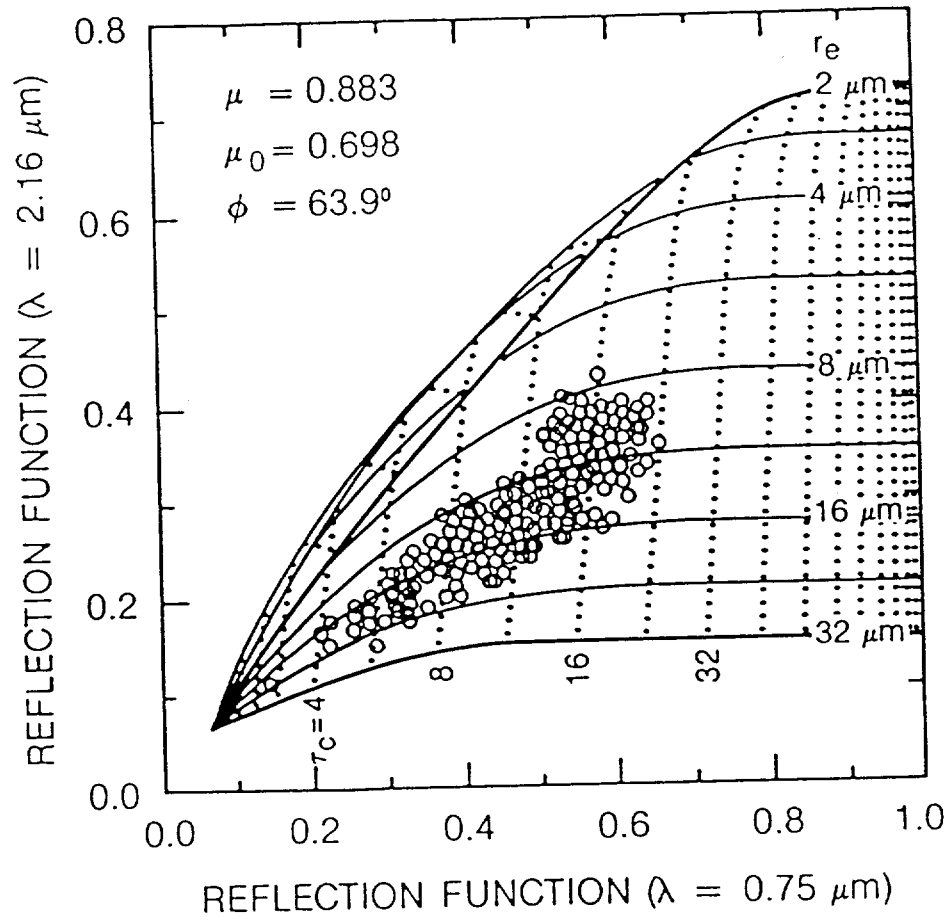


Figure 2

MAXIMUM LIKELIHOOD ESTIMATION (MLE) SCENE IDENTIFICATION ALGORITHM

Introduction to MLE

The Maximum Likelihood Estimation (MLE) scene identification technique is a statistical scene identification algorithm that is presently being used by the Earth Radiation Budget Experiment (ERBE) project, for processing the Nimbus-7 ERB scanner measurements to produce improved ERB products and in the NOAA/NESDIS Earth Radiation Budget Instrument (ERBI) system simulation study. The Cloud and Earth Radiant Energy System (CERES) team will probably require MLE-derived scene type estimates for the generation of its standard Earth radiation budget products. These estimates will be generated either by the CERES team at the IFOVs of their instrument, or by the MODIS team at higher spatial resolution.

Basic Algorithm

Identify the geographic surface type for the region. At least the following surfaces will be considered: Ocean, Land, Snow, Desert, and Land/Ocean (coastal).

The cloud cover estimate is determined using statistics from a bivariate normal distribution. The MLE procedure determines the fractional cloud cover for each longwave/shortwave radiance pair. The MLE algorithm will be capable of selecting one of four possible cloud amounts. When these cloud amounts are combined with the five geographic surface types, the following cloud/geography scene types are possible:

- | | |
|------------------------|----------------------------------|
| 1. Clear/Ocean | 7. Partly Cloudy/Land or Desert |
| 2. Clear/Land | 8. Partly Cloudy/Land-Ocean Mix |
| 3. Clear/Snow | 9. Mostly Cloudy/Ocean |
| 4. Clear/Desert | 10. Mostly Cloudy/Land or Desert |
| 5. Clear/Land-Ocean | 11. Mostly Cloudy/Land-Ocean Mix |
| 6. Partly Cloudy/Ocean | 12. Fully Overcast |

The twelve basic shortwave bidirectional reflectance models are global in application and refer to all seasons. For each of the twelve scenes, there is a directional model which specifies how the albedo varies with solar zenith angle. The longwave limb darkening models are divided into ten latitude bands, each 18° in width, and four seasons (winter, spring, summer, and fall).

From each set of radiance observations (longwave and shortwave), choose the appropriate set of ERBE cloud statistics based on the geographic surface type for the region. For example, if the surface is land, then select the set of statistics for the appropriate cloud/geography types 2, 7, 10, and 12.

The probability that a particular cloud cover produces the scanner shortwave radiance measurement, M_{SW} , and longwave radiance measurement, M_{LW} , is given by:

$$P_c = \frac{1}{2\pi\sigma_c(SW)\sigma_c(LW)(1-r_c^2)^{1/2}} e^{-G/2}$$

where

$$G = \frac{1}{(1-r_c^2)}$$

$$\left\{ \left[\frac{M_{SW} - L_c(SW)}{\sigma_c(SW)} \right]^2 - 2r_c \left[\frac{(M_{SW} - L_c(SW)) (M_{LW} - L_c(LW))}{\sigma_c(SW) \sigma_c(LW)} \right] + \left[\frac{M_{LW} - L_c(LW)}{\sigma_c(LW)} \right]^2 \right\}$$

c = cloud/geography type

M_{LW} = mean longwave radiance

M_{SW} = mean shortwave radiance

ϕ = satellite zenith angle

y = relative azimuth angle

μ_o' = cosine of the solar zenith angle

θ = latitude

(ϕ, y) = angular bin (1-49)

t = time, season

$\sigma_c(SW)$ = standard deviation of the elements of a shortwave bidirectional model;
f(c, m_o' , (ϕ, y))

$\sigma_c(LW)$ = standard deviation of the elements of a longwave anisotropic model;
f(c, ϕ, θ, t)

r_c = correlation coefficient between shortwave and longwave radiances for
each angular bin of the shortwave model; f(c, m_o' , (ϕ, y))

$$L_c(SW) = \frac{1}{\pi} S_o l(t) \mu_o' \hat{a}_c R_c$$

S_o = solar constant

l(t) = reciprocal of the E-S distance squared

μ_o' = cosine SZA

\hat{a}_c = estimated albedo; f(c, m_o')

R_c = bidirectional shortwave model; f(c, m_o' , (ϕ, y))

$$L_c(LW) = \frac{1}{\pi} \hat{M}_c A_c$$

\hat{M}_c = estimated longwave exitance for a cloud/geography type c

A_c = longwave anisotropic model value; f(c, ϕ, θ)

Calculate the appropriate four probabilities (P_c) for each cloud/geography type. Initially assume that the correlation between the longwave and shortwave radiances is zero. The probability equations can then be written as:

$$P_c = \frac{1}{2\pi\sigma_c(\text{SW})\sigma_c(\text{LW})} e^{-G/2}$$

$$G = \left[\frac{M_{\text{SW}} - L_c(\text{SW})}{\sigma_c(\text{SW})} \right]^2 + \left[\frac{M_{\text{LW}} - L_c(\text{LW})}{\sigma_c(\text{LW})} \right]^2$$

The probability equation can be rewritten as follows for the special cases when there is only one radiance measurement available:

Shortwave radiance only, M_{SW} :

$$P_c = \frac{1}{\sigma_c(\text{SW})\sqrt{2}\pi} e^{-G/2}$$

$$G = \left[\frac{M_{\text{SW}} - L_c(\text{SW})}{\sigma_c(\text{SW})} \right]^2$$

Longwave radiance only, M_{LW} :

$$P_c = \frac{1}{\sigma_c(\text{LW})\sqrt{2}\pi} e^{-G/2}$$

$$G = \left[\frac{M_{\text{LW}} - L_c(\text{LW})}{\sigma_c(\text{LW})} \right]^2$$

After calculating the four probabilities (P_c), select the cloud amount based on the largest probability obtained.

From the cloud type determined in Step 7, select the appropriate bidirectional shortwave model and longwave exitance model.

Using these models, estimate the albedo, shortwave flux, and longwave flux for the sub-TA.

Tuning of Basic MLE Algorithm/Models

The software bidirectional reflectances are given for ten solar zenith angles, seven satellite zenith angle bins, and eight azimuth bins. Linear interpolation is done over the satellite zenith and azimuth angles and the solar zenith angles

to obtain a smooth transition from one bin to the next.

The longwave limb darkening values are given for seven satellite azimuth bins, ten latitude bands, and four seasons. Bilinear interpolation is done over azimuth and latitude band areas to provide a smooth variation, but no seasonal interpolation is performed.

Each shortwave and longwave anisotropic model has associated with it a longwave (W/m^2) model value and an albedo. The longwave models, of course, vary with latitude band and with the season.

The ERBE inversion system has also utilized a set of longwave flux models for nighttime. An empirical model was developed to compute a nighttime longwave modelled flux. Surface dependent adjustment factors are subtracted from the daytime longwave fluxes as a function of geography to obtain the nighttime fluxes. These exact adjustments were assumed to be valid only when the Sun was overhead at the latitude of the target. The correction then varies as a function of the cosine of the difference between the Sun declination and the latitude of the target.

$$LW \text{ Night Flux} = LW \text{ Day Flux} - (\text{Day-Night}) * \cos (\phi_{\text{target}} - \phi_{\text{sun}})$$

where ϕ = latitude

In a few cases, the original MLE algorithm classified hot dark regions as overcast. This usually occurred for pixels which were considerably warmer than the model longwave flux TA value. To prevent this, a dark/hot threshold was set up. Thus, any radiance observations for which $M_{SW} < L_{SW}^{CLR} - 2 \sigma_{SW}^{CLR}$ or $M_{LW} > L_{LW}^{CLR} + \sigma_{LW}^{CLR}$ are classified as clear.

Studies by the ERBE Team indicated that setting the (SW, LW) correlation factor $r_c(SW, LW) = 0$ produced no change in the total flux calculations and only a marginal change in the ability to identify clear scenes. Therefore, they run their production model without the $r_c(SW, LW)$ term.

To improve clear scene identification, the ERBE Team introduced a priori probabilities for a scene being clear, partly cloudy, mostly cloudy, or overcast. These probabilities were basically derived from the Nimbus-7 NCLE cloud data set on a zonal and seasonal basis. Linear interpolation is used from zone to zone.

If all the probabilities are quite small, it can be assumed that the models are not very applicable to the scene in question, and, hence, the results are very questionable. Define $d_{SW} = [(M_{SW} - L_c(SW))/\sigma_c(SW)]^2$ and $d_{LW} = [(M_{LW} - L_c(LW))/\sigma_c(LW)]^2$.

The ERBE algorithm rejects a pixel if $d_{min} > N = 8\sigma_c$, where $d = d_{SW} + d_{LW}$ and where d_{min} corresponds to the largest probability of (clr, pc, mc, o), and c is an index indicating one of the four cases.

If one of the model shortwave anisotropic factors for a particular measurement

is large, then the MLE derived flux may become double valued with one flux value much larger than the other. An example is a measurement over the ocean which lies in a clear ocean sunglint region. The shortwave measurement is large but MLE may show nearly equal probability for clear ocean and overcast. The calculated inverted fluxes may vary by a factor of 2 or 3. If low clouds are involved, then the longwave measurement will not act as a useful discriminator. To reject such ambiguous cases, the ERBE Team rejects measurements where one of the applicable model anisotropic factors is $> R^*$. They recommend that $R^* = 2$.

The ERBE Team rejects pixels with associated satellite zenith angles greater than 70° . There are two reasons for this. The ERBE footprint becomes very large at large satellite zenith angles. This causes confusion in both scene identification and target area designation. Some evidence indicates that the combined (ERBE models/MLE algorithm) are more ambiguous and less accurate at large satellite zenith angles.

References

Wielicki, B. A. and R. N. Green, 1989: Cloud Identification for ERBE Radiative Flux Retrieval. J. Appl. Meteor., 28, In Press.

Kyle, H. L., personal communication--The principal source for this material.

WATER LEAVING (MODIS-ERA) RADIANCE ALGORITHM

Introduction

Atmospheric correction involves removing the contributions of the atmosphere from the total radiance signal received by the satellite, thereby revealing the water-leaving radiance contribution. Removal of atmospheric contributions is critical for ocean products because the atmosphere accounts for about 90% of the signal received at the satellite.

Despite having only four visible bands and relatively poor radiometric sensitivity, the CZCS was able to generate water-leaving radiances within about 10% (Gordon et al., 1983). With a large spectral suite of bands and higher radiometric sensitivity, MODIS can be expected to improve on the CZCS performance, and subsequently generate more accurate chlorophyll concentrations. The key to the MODIS atmospheric correction is the presence of bands in the near IR, where the water-leaving radiance may be assumed zero, allowing a pixel-by-pixel removal of aerosols.

Nevertheless, the CZCS experience provides the basis for an atmospheric correction for MODIS. The principle of atmospheric correction remains the same

$$L_t(\lambda) = L_r(\lambda) + L_a(\lambda) + L_g(\lambda) + t(\lambda)L_w(\lambda) \quad (1)$$

where $L_t(\lambda)$ is the total radiance received by the sensor, $L_r(\lambda)$ is the contribution arising from Rayleigh scattering, $L_a(\lambda)$ is that arising from aerosol scattering, $L_g(\lambda)$ is the contribution from sun glitter (direct sunlight reflecting from the sea surface), and $t(\lambda)L_w(\lambda)$ is the water-leaving radiance $L_w(\lambda)$ diffusely transmitted to the top of the atmosphere $t(\lambda)$. Eqn. 1 is identical to the algorithm used for CZCS atmospheric correction except for the addition of a correction for sun glitter.

Irradiance

The procedure for atmospheric correction for MODIS begins with obtaining, from literature values (Neckel and Labs, 1984), the mean extraterrestrial solar irradiance E_o , which must be weighted for MODIS bandwidths and bandwidth sensitivity. Then the instantaneous extraterrestrial solar irradiance F_o must be computed

$$F_o(\lambda) = E_o(\lambda)[1 + e \cos[2\pi(JD-3)/365]]^2 \quad (2)$$

(Gordon et al., 1983) where e is the eccentricity of the Earth's orbit (= 0.016) and JD is Julian Day.

Filter

Further processing requires that only cloud-free pixels be identified, so a method for identifying cloudy pixels will be employed. The CZCS uses a threshold radiance value at 750 nm, and it is assumed MODIS will use the same approach.

Once the cloud-free pixels have been identified, they must be Earth-located so that solar and spacecraft zenith and azimuth angles may be computed.

Absorption

With zenith and azimuth angles known, one must next obtain the ozone optical thickness $\tau_{oz}(\lambda)$. Gordon (1989) proposes using GOMR data for ozone optical thickness, but other sources may be available, including MODIS itself. AIRS/AMSU may also provide a source of ozone information.

Next is calculated the instantaneous solar irradiance after reduction by two passes through the ozone layer

$$F_o'(\lambda) = F_o(\lambda) \exp[-\tau_{oz}(\lambda) (1/\cos\theta + 1/\cos\theta_o)] \quad (3)$$

where θ is the spacecraft zenith angle and θ_o is the solar zenith angle.

Radiances

The contribution to the satellite from Rayleigh scattering must then be removed. This is computed by including multiple scattering effects and polarization (Gordon et al., 1988). On the CZCS this is computed every 8 pixels across a scan line and every 16 scan lines. Values between these points are computed by bi-linear interpolation.

First the Rayleigh optical thickness $\tau_r(\lambda)$ must be computed. Assuming a depolarization factor of 0.031 (Gordon et al., 1988), a "standard" Rayleigh optical thickness $\tau_{ro}(\lambda)$ (at standard atmospheric pressure P_o , 1013.25 mbar) may be computed by

$$\tau_{ro}(\lambda) = 0.008569\lambda^{-4}(1 + 0.0113\lambda^{-2} + 0.00013\lambda^{-4}) \quad (4)$$

(Hansen and Travis, 1974). $\tau_r(\lambda)$ may then be calculated at any surface pressure P by

$$\tau_r(\lambda) = P/P_o \tau_{ro}(\lambda) \quad (5)$$

The surface atmospheric pressure field at low resolution may be obtained from meteorological data and models from NOAA.

The total intensity of multiple scattered Rayleigh radiance, I , normalized to unit incoming solar irradiance, may then be computed from

$$I(\tau_r(\lambda), \theta, \theta_o, \Delta\phi) = \sum_{m=0,2} I_m(\tau_r(\lambda), \theta, \theta_o) \cos(m\Delta\phi) \quad (6)$$

where I_m are Fourier coefficients of the radiance and $\Delta\phi = \phi - \phi_o$ where ϕ and ϕ_o are the spacecraft and solar azimuth angles, respectively. For the CZCS, the Fourier coefficients I_m are computed in advance for a fixed Rayleigh optical thickness. They are made available for CZCS processing at 40 spacecraft zenith angles and 39 solar zenith angles. Interpolation to other combinations of angles

is done by bilinear interpolation. Rayleigh radiance $L_r(\lambda)$ is then $I(\lambda) F_o'(\lambda)$.

For MODIS, the Fourier coefficients I_m will also be computed in advance, except that they will include a surface pressure dependence in addition to the spacecraft and solar zenith angle dependence, producing a look-up table of three variables. The normalized Rayleigh radiance intensities I will then be interpolated from this look-up table, and multiplied by $F_o'(\lambda)$ to obtain $L_r(\lambda)$.

Correction for Sun Glitter

The tilt capability of MODIS-T drastically reduces the amount of sun glitter contribution to the total radiance. However, minor amounts of sun glitter are commonly present, even on sensors with a tilt capability. These contributions are usually absorbed into the estimation of the aerosol and are corrected along with aerosols. However, at times the sun glitter may be more intense, and a method for removal will facilitate more accurate water-leaving radiance computations. Furthermore, MODIS-N has no tilt capability, and the sun glitter contribution to its total radiance signal may be significant at times.

Sun glitter is known to be related to the wind speed. Knowledge of the wind speed enables an estimation of the sea slope probability distribution, which determines the intensity of sun glitter.

Two methods are proposed by Gordon for the removal of sun glitter from MODIS imagery. The first is to obtain surface wind velocities from SCATT-2 to determine the distribution of surface sea slopes according to the Cox and Munk (1954) theory. The glitter radiance can then be determined from the slope distribution and orbital geometry. If SCATT-2 winds are not available, surface wind velocities may be estimated from meteorological models. The second is to obtain glitter radiance from land bands on MODIS-N, and estimate the surface sea slope distribution therefrom. Again the glitter radiance can be estimated from these slopes and orbital geometry.

This correction can only be attempted for weak sun glitter, i.e., at the edges of intense glitter. In areas of intense sun glitter no correction is possible. Determining where this correction can apply may require human intervention since sun glitter patterns are usually determined by visual inspection. However, it may be possible to automate this procedure, and Gordon will run simulations to assess this possibility.

Aerosol Radiances

Correction for aerosol scattering and absorption for MODIS takes advantage of the fact that water is totally absorbing for $\lambda > 660$ nm in Case 1 waters, except near 685 nm where chlorophyll fluoresces. Thus, from Eqn. 1, $L_a(\lambda)$ is known for these wavelengths after Rayleigh radiance and sun glitter removal. $S(\lambda_1, \lambda_2)$ is the ratio of aerosol radiances at two wavelengths

$$S(\lambda_1, \lambda_2) = L_a(\lambda_1)/L_a(\lambda_2) \quad (7)$$

and may be computed directly at those wavelengths where $L_a(\lambda)$ may be determined directly from Eqn. 1, assuming no sun glitter. $S(\lambda_1, \lambda_2)$ is related to a parameter $\epsilon(\lambda_1, \lambda_2)$ which is essentially the ratio of the aerosol optical thicknesses at these two wavelengths

$$\epsilon(\lambda_1, \lambda_2) = S(\lambda_1, \lambda_2) F_o'(\lambda_2)/F_o'\lambda_1 \quad (8)$$

where $F_o(\lambda)$ is the instantaneous extraterrestrial irradiance corrected for two trips through the ozone layer (Eqn. 3).

The utility of Eqn. 8 is that if ϵ can be determined for all wavelengths, then the aerosol radiances at all wavelengths may be determined by computing S and then multiplying S by the known aerosol radiance at a wavelength where water is totally absorbing, e.g. at 865 nm

$$L_a(\lambda_i) = S(\lambda_i, \lambda_{865}) L_a(\lambda_{865}) \quad (9)$$

Substituting Eqn. 9 into Eqn. 1

$$L_w(\lambda) = [L_t(\lambda) - L_r(\lambda) - L_g(\lambda) - S(\lambda, \lambda_{865})L_a(\lambda_{865})]/t(\lambda) \quad (10)$$

Gordon (1989) proposes the following approach for determining ϵ for MODIS.

Let λ_o be a MODIS wavelength at which water is always (even in Case 2 waters) totally absorbing; 875 nm on MODIS-T or 865 nm on MODIS-N. For Case 1 waters the water-leaving radiance near 665 nm should be zero, as will the water-leaving radiance at 755 or 750 nm for all waters. At these wavelengths we know ϵ from knowledge of S and Eqn. 8. We seek ϵ at wavelengths for which the water-leaving radiance is non-zero, all the way into the blue at 410 nm. Using an Angstrom approximation, and assuming ϵ represents the ratio of aerosol optical thicknesses at two wavelengths, we assume

$$\epsilon(\lambda_i, \lambda_o) = (\lambda_i/\lambda_o)^{\eta(\lambda_i)} \quad (11)$$

where the subscript i refers to 665 nm and 755 (or 750) nm. We generate two $\eta(\lambda_i)$'s using the ratios of $\lambda(665)$ and $\lambda(750)$ to λ_o . The method of extrapolation of these $\eta(\lambda_i)$'s to shorter wavelengths is undetermined, but for the CZCS it was assumed that η of shorter wavelengths was the mean of the η 's at higher wavelengths. Thus,

$$\eta(\lambda_i) = (\eta(\lambda_{665}) + \eta(\lambda_{750}))/2 \quad (12)$$

We can now compute $\epsilon(\lambda_i, \lambda_o)$ for i = all wavelengths from Eqn. 11 and then $S(\lambda_i, \lambda_o)$ from Eqn. 8. Since $L_a(865)$ is known, $L_a(\lambda_i)$ is known from Eqn. 7. The important point here is that, unlike the CZCS, the aerosol type (characterized by ϵ) can be determined at each pixel, thus minimizing errors associated with assuming a constant aerosol type in an entire scene. For Case 2 waters, Eqn. 12 cannot be used because $L_w(665)$ is not necessarily zero. In such case, either the η computed using only the 750 band will have to be used, or some other method sought.

Determination of the aerosol radiances is subject to three fundamental assumptions: 1) that the water-leaving radiance is zero for $\lambda > 660$ nm, 2) that the aerosols follow the Angstrom wavelength dependence, and 3) that the aerosol optical thickness is < 0.6 . The first of these assumptions is validated by observation, except in the cases of significant suspended sediment, coccolithophores, or chlorophyll fluorescence, for which significant water-leaving radiance between 660 and 690 nm may be present. Usually these waters will be classified as Case 2 and extrapolation of Angstrom exponents will have to be made based on the exponent determined for $\lambda_{750}/\lambda_{865}$ (i.e., assumed spectrally constant). Such waters, however, usually constitute $< 10\%$ of the oceanic area. The second assumption, that Angstrom's formulation is valid, may be suspect in some instances, but generally it has been found to be representative for most aerosols. The third assumption, that $\tau_a(\lambda)$ be < 0.6 , is usually ensured through the cloud-flagging process, which removes from processing not only cloudy pixels, but also those with large haze concentrations.

Water-Leaving Radiances

All terms in Eqn. 1 are now known except $t(\lambda)$ and $L_w(\lambda)$. The water-leaving radiance will be revealed once $t(\lambda)$, the diffuse atmospheric transmittance is computed. The expression is

$$t(\lambda) = \exp[-(\tau_r(\lambda)/2 + \tau_{oz}(\lambda))]/\cos\theta \quad (13)$$

where $\tau_r(\lambda)$ is the Rayleigh optical thickness and $\tau_{oz}(\lambda)$ is the ozone optical thickness. Eqn. 1 may now be solved for $L_w(\lambda)$.

The method for computing $L_w(\lambda)$ (i.e., correcting the radiance signal for atmospheric contributions) for MODIS is substantially simpler than for the CZCS. This is because the Near IR bands on MODIS will allow a pixel-by-pixel estimation of aerosol radiance, and avoid the required assumption in the CZCS that the aerosol type does not change substantially over a scene. This pixel-by-pixel aerosol correction will also improve the accuracy of water-leaving radiance from MODIS, which for the CZCS was $\approx 10\%$, thereby allowing more accurate estimates of pigment concentrations. However, although the MODIS atmospheric correction algorithm is simpler in design, it requires substantially more computations per pixel than the CZCS.

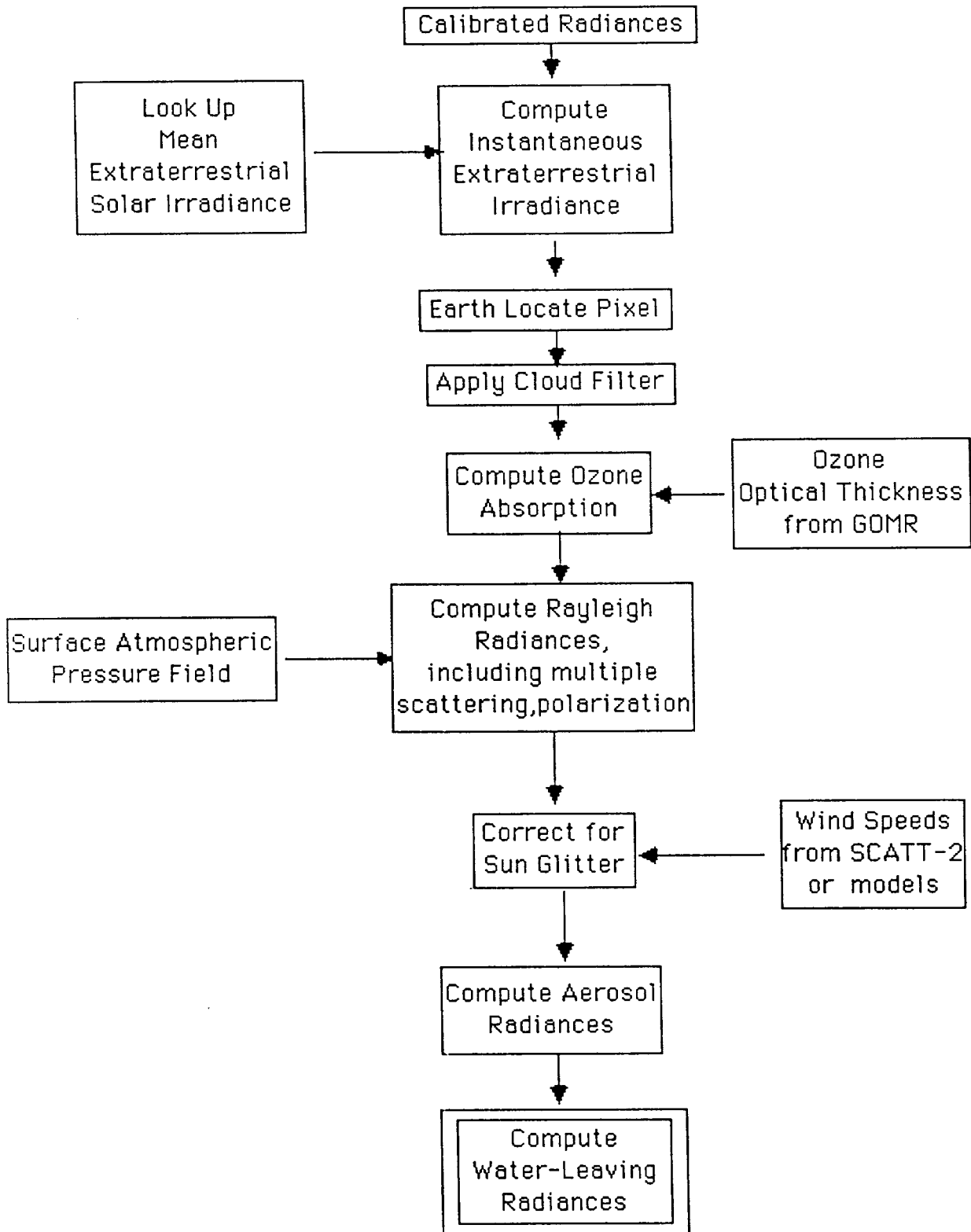
References

- Cox, C. and W. Munk, 1954. Measurement of the roughness of the sea surface from photographs of the sun's glitter. *J. Mar. Res.* 44: 838-850.
- Gordon, H.R., 1989. Algorithm development for ocean observation with EOS/MODIS. MODIS Science Team Member Report.
- Gordon, H.R., D.K. Clark, J.W. Brown, O.B. Brown, R.H. Evans, and W.W. Broenkow, 1983. Phytoplankton pigment concentrations in the Middle Atlantic Bight: comparison of ship determinations and CZCS estimates. *Applied Optics* 22: 20-

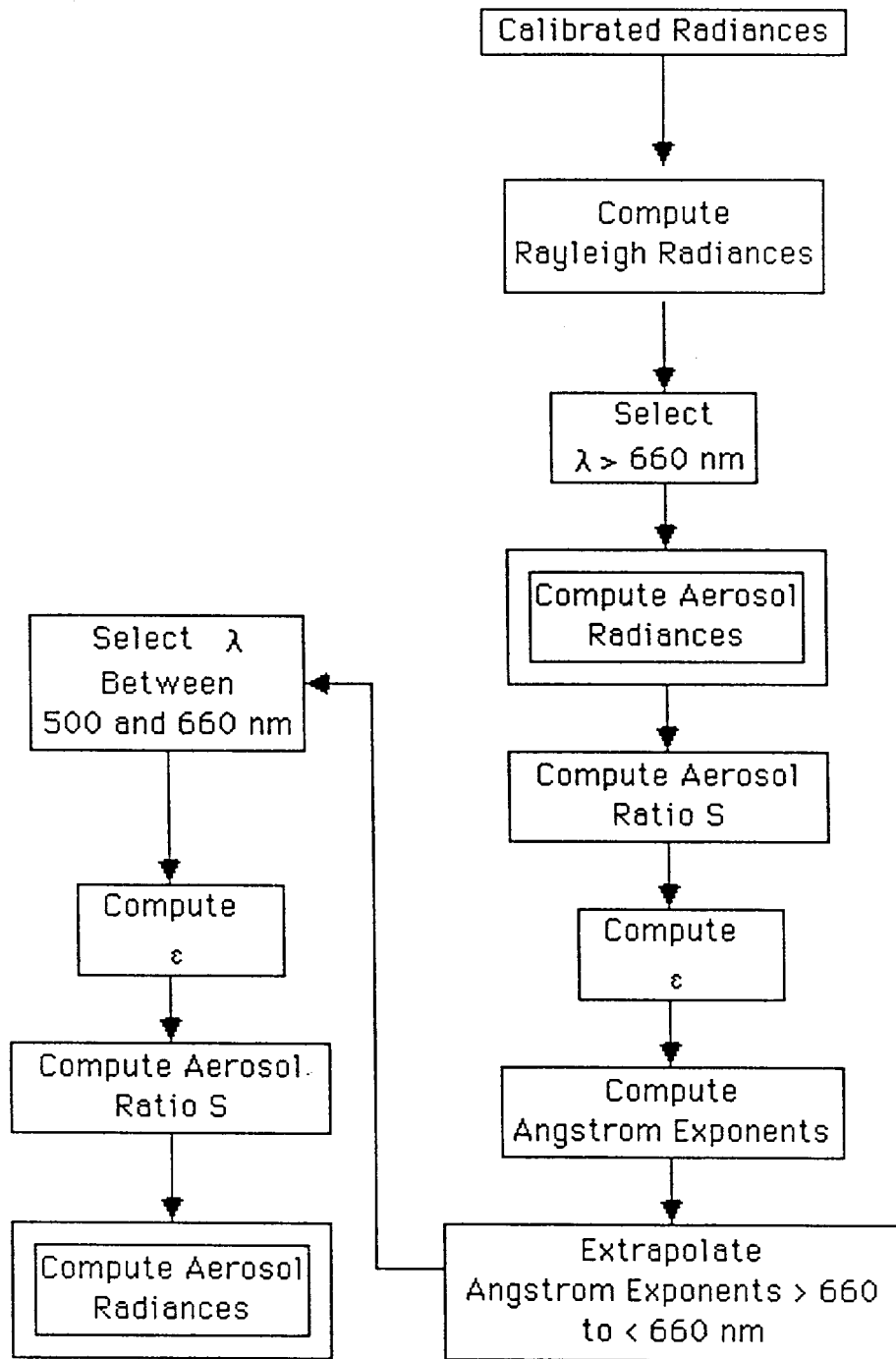
36.

Hansen, J.E. and L.D. Travis, 1974. Light scattering in planetary atmospheres. Space Sci. Rev. 16: 527.

Atmospheric Correction
to Determine Water-Leaving Radiances
for MODIS



Determination of
Single-Scattering Aerosol Radiances



CASE-2 WATERS CHLOROPHYLL-A PIGMENT CONCENTRATION

Introduction

According to the optical classification by Morel and Prieur (1977), oceanic waters may be characterized as Case 1, in which the optical properties are dominated by chlorophyll and associated (and covarying) detrital pigments, or as Case 2, in which other substances (primarily dissolved organic matter, known as gelbstoff or yellow substances, suspended sediments, and detached coccoliths) which do not covary with chlorophyll also affect the optical properties. Pigment retrievals from the CZCS in Case 1 waters (which comprise the vast majority of the world's oceans) have achieved reasonable success ($\pm 30\%$; Gordon et al., 1983). However, the non-chlorophyll-covarying "other substances" in Case 2 waters have hampered the retrieval of accurate estimates of pigment concentrations in these waters, producing errors up to a factor of three (Carder, 1989).

One of the most prevalent "other substances" in Case 2 waters is gelbstoff, which is a refractory, high molecular weight organic compound derived from the degradation of chlorophyll of both oceanic and terrestrial origin. Although absorption by gelbstoff has a markedly different spectral shape than absorption by chlorophyll (particularly in the blue end (400-440 nm) of the spectrum), it could not be separated from the signal seen by the CZCS because of a lack of spectral bands in this region. Such is not the case with MODIS, which contains a sufficient number of spectral bands and in the correct locations (i.e., 413 nm on MODIS-N; 410 and 425 nm on MODIS-T) to allow, in principle, the separation of gelbstoff from pigment concentrations. This should allow improved chlorophyll estimates from MODIS over the CZCS.

Selection Procedure

Dr. Ken Carder proposes pre-launch core data products to enable determination of chlorophyll in Case 2 waters in which gelbstoff plays an important optical role. A flag-type algorithm will separate Case 1 from Case 2 waters to prevent redundant processing. This algorithm will use excess gelbstoff per unit chlorophyll as a flag for Case 2 waters where the Case 1 algorithm breaks down. From data already collected, a gelbstoff: chlorophyll concentration ratio of 10:1 appears to mark the onset of the breakdown of the Case 1 algorithm.

Upon locating Case 2 waters from the flag algorithm, processing for Case 2 chlorophyll concentrations will begin. At present, the proposed algorithm deals only with the deconvolvement of chlorophyll from gelbstoff; inclusion and separation of detached coccoliths and suspended sediments is a proposed research activity. The principle is as follows.

Estimation Algorithm

The spectral remote-sensing reflectance R_{RS} (that viewed from above the water) is defined as

$$R_{RS}(\lambda) = \pi I_w(\lambda) / E_d(\lambda, 0) \quad (1)$$

(Carder and Steward, 1985) where $L_w(\lambda)$ is the water-leaving radiance, and $E_d(\lambda, 0)$ is the downwelling irradiance at the sea surface. R_{RS} may also be related to inherent optical properties of the water

$$R_{RS}(\lambda) = 0.1076 b_b(\lambda)/a(\lambda) \quad (2)$$

where $b_b(\lambda)$ is the backscattering coefficient of the constituents in the water (and the water itself) and $a(\lambda)$ is the absorption coefficient. Since b_b and a are inherent optical properties, they may be expanded to include contributions by various constituents

$$b_b = b_{bw} + b_{bc} \quad (3)$$

and

$$a = a_w + a_c + a_g \quad (4)$$

(λ -dependence has been dropped) where the subscript w represents the contribution by water, c represents that by chlorophyll, and g represents that by gelbstoff.

Now b_{bw} is known a priori from Morel (1974) and a_w from Smith and Baker (1981). b_{bc} and a_c may be expressed in terms of chlorophyll concentrations and a_g may be expressed in terms of gelbstoff concentration (Carder, 1989). Thus, we have two unknowns in one equation (Eqn. 2).

Carder (1989) has derived a look-up table generated by iterating on various combinations of chlorophyll and gelbstoff concentrations, and their result on water-leaving radiance ratios (Figure 1). From knowledge of the ratio of $L_w(412)/L_w(443)$ to the logarithm of the ratio of $L_w(443)/L_w(565)$, obtainable by the satellite, one can estimate the concentrations of chlorophyll and gelbstoff using a look-up table (Figure 1). So the algorithm is to compute the ratios $L_w(412)/L_w(443)$ and the log [$L_w(443)/L_w(565)$] and use the look-up table to estimate chlorophyll.

The method has only been tested for oceanic regions with $< 2 \text{ mg m}^{-3}$ chlorophyll concentrations, but has reduced the error from $> 400\%$ in some cases to $\pm 50\%$. This look-up table would be made available to EosDIS, and requires only water-leaving radiances as input. A method of interpolation will be required to generate output from this look-up table.

The algorithm will apply only to pre-determined Case 2 waters, an estimated 10% of the total cloud-free pixels. It also applies only to suspended sediment-free waters. Carder proposes to develop algorithms for waters containing significant sediment backscatter, but this is a research effort and not a core data product.

References

Carder, K.L. and R.G. Steward, 1985. A remote-sensing reflectance model of a red-tide dinoflagellate off west Florida. *Limnology and Oceanography* 30: 286-298.

Carder, K.L. 1989. High spectral resolution MODIS-T algorithms for ocean chlorophyll in Case II waters. Eos Team Member Proposal.

Morel, A., 1974. Optical properties of pure water and seawater. pp. 1-24. In: Optical aspects of oceanography, N.G. Jerlov and E. Steeman-Nielsen, eds. Academic Press.

Morel, A. and Prieur, L., 1977. Analysis of variations in ocean color. Limnology and Oceanography 22: 709-722.

Smith, R.C. and K.S. Baker, 1981. Optical properties of the clearest natural waters (200-800 nm). Applied Optics 20: 177-184.

Determination of Pigment Concentrations
in Case 2 Waters

